ACS OMEGA

http://pubs.acs.org/journal/acsodf

Article

WaterMap and Molecular Dynamic Simulation-Guided Discovery of Potential PAK1 Inhibitors Using Repurposing Approaches

Jayashree Biswal, Prajisha Jayaprakash, Suresh Kumar Rayala, Ganesh Venkatraman, Raghu Rangaswamy, and Jeyakanthan Jeyaraman*

Cite This: *ACS Omega* 2021, 6, 26829−26845

Read Online

ACCESS | Metrics & More | Article Recommendations | Supporting Information

ABSTRACT: p21-Activated kinase 1 (PAK1) is positioned at the nexus of several oncogenic signaling pathways. Currently, there are no approved inhibitors for disabling the transfer of phosphate in the active site directly, as they are limited by lower affinity, and poor kinase selectivity. In this work, a repurposing study utilizing FDA-approved drugs from the DrugBank database was pursued with an initial selection of 27 molecules out of ∼2162 drug molecules, based on their docking energies and molecular interaction patterns. From the molecules that were considered for WaterMap analysis, seven molecules, namely, Mitoxantrone, Labetalol, Acalabrutinib, Sacubitril, Flubendazole, Trazodone, and Niraparib, ascertained the ability to overlap with high-energy hydration sites. Considering many other displaced unfavorable water molecules, only Acalabrutinib, Flubendazole, and Trazodone molecules highlighted their prominence in terms of binding affinity gains through $\Delta\Delta G$ that ranges between 6.44 and 2.59 kcal/mol. Even if Mitoxantrone exhibited the highest docking score and greater interaction strength, it did not comply with the WaterMap and molecular dynamics simulation results. Moreover, detailed MD simulation trajectory analyses suggested that the drug molecules Flubendazole, Niraparib, and Acalabrutinib were highly stable, observed from their RMSD values and consistent interaction pattern with Glu315, Glu345, Leu347, and Asp407 including the hydrophobic interactions maintained in the three replicates. However, the drug molecule Trazodone displayed a loss of crucial interaction with Leu347, which was essential to inhibit the kinase activity of PAK1. The molecular orbital and electrostatic potential analyses elucidated the reactivity and strong complementarity potentials of the drug molecules in the binding pocket of PAK1. Therefore, the CADD-based reposition efforts, reported in this work, helped in the successful identification of new PAK1 inhibitors that requires further investigation by *in vitro* analysis.

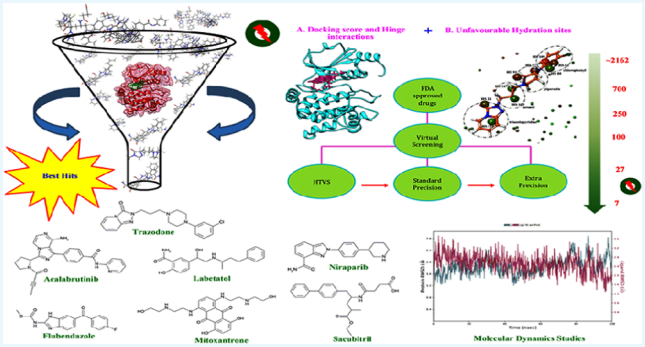

INTRODUCTION

The prevalence and incidence of cancer have escalated to over 18.1 million cases, and there have been 9.6 million deaths according to a 2018 report by the International Agency for Research and Cancer (IARC).[1,2] According to the human development index (HDI), about 52% of the global total, 10.6 million cases are likely to occur in low- to medium-income countries by 2030.[3] Cancers in the lungs, breast, pancreas, stomach, and colorectal are known to be the lethal cancer types, in terms of mortality, with limited therapeutic options.[2] The occurrence of tumor heterogeneity, chemoresistance, and aggressive metastasis, and lack of effective treatments toward relapsed cancers have affected clinical benefits and response rates in cancer patients.[2] Furthermore, the conventional drug discovery process for cancer therapeutics is both expansive and expensive, with a low success rate of more than 70% failures in phase II or phase III clinical trials.[4−7] These factors are the main challenges in the development of effective cancer agents.

Generally, drug repurposing, which is otherwise known as drug repositioning, refers to the identification of new therapeutic applications for the existing and investigational drugs.[8−11] In such instances, antiviral (Gemcitabine, Nelfinavir),[12,13] anticonvulsant (Valproic acid),[14] antifungal (Itraconazole),[15] osteoporosis (Raloxifene),[16] and other noncancer drugs like Thalidomide,[17,18] Aspirin,[19,20] Celecoxib,[21] Metformin,[22] Digoxin,[23] Nitroxoline,[24] etc. have been successfully repurposed with proven mechanism of action[2,25−28] in the treatment of cancer. Despite varied advantages of drug repurposing, clinical translations of repurposed drug have been limited by sufficient target tissue concentrations,[29]

Received: April 16, 2021
Published: October 5, 2021

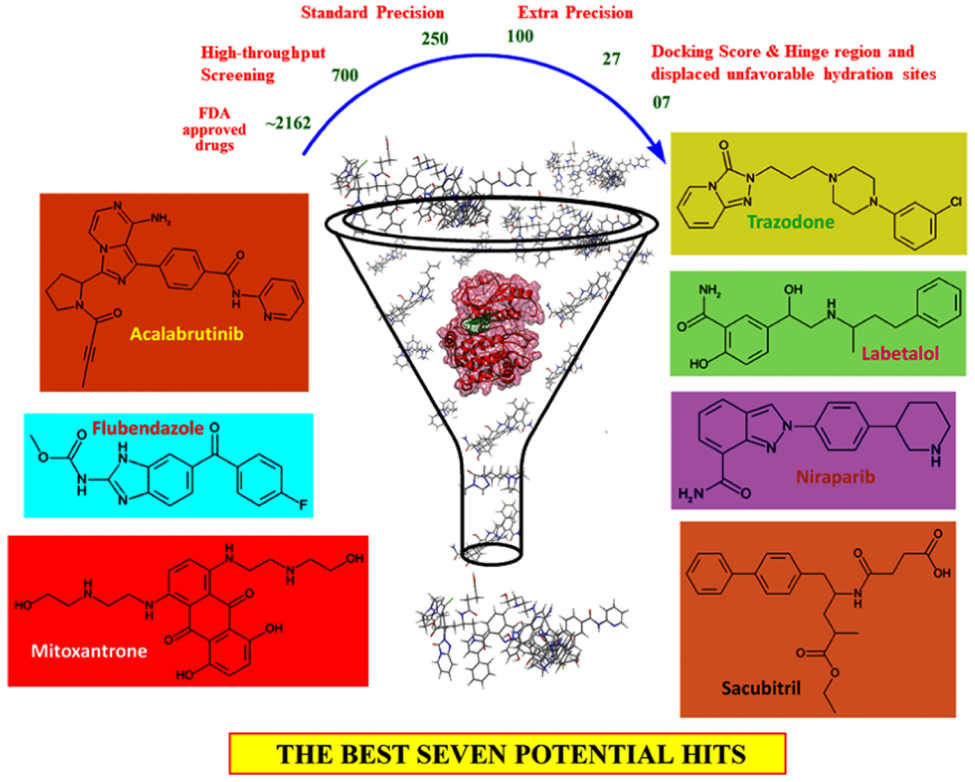

Figure 1. Schematic illustration of the structure-based virtual screening for the discovery of potential PAK1 inhibitors.

efficacy in phase II and phase III clinical trials,[30] and undefined regulatory guidelines.[32] Thus, by sharing the same pharmacological target-binding site or pathway, the approved drugs have varying noncanonical target profiles, and they display a range of unintended applications.[31] Nonetheless, owing to the unprecedented accumulation of biological and molecular data on mechanisms and pathways for inducing cancer, a coherent application of bioinformatics tools can offer a better paradigm for a promising anticancer drug discovery.[25]

The kinase phosphorylation process is instrumental in the regulation of cellular activities that includes proliferation, survival, apoptosis, metabolism, etc., *via* mediating signal transduction pathways.[33] The deregulation of cellular responses has resulted in an onset of pathological responses, and hence kinases are considered as a pioneering drug target class for the treatment of various clinical manifestations.[34] To date, there are approximately 30 FDA-approved small-molecule kinase inhibitors for 518 human kinases, which represent about one-fifth of the human kinome.[35,36]

Group-I p21-activated kinase 1 (PAK1), a serine/threonine protein kinase, was downregulated by the interaction with the Ras-related Rho family GTPases Cdc42/Rac1. This resulted in disrupted dimerization and auto-inhibitory domain (AID) dissociation, which expedited PAK1 activation.[37,107] Besides, the conformational rearrangements facilitating the autophosphorylation of Thr423 in PAK1, which is a crucial phosphorylation site involved in the inhibition of AID binding and stabilization of the activation segment of phosphorylation.[38] Like other kinases, PAK1 is essential for various cellular functions such as cytoskeletal organization, motility, mitosis, and angiogenesis. These roles make them attractive therapeutic targets for cancer,[39] infectious diseases, and neurological disorders.[40] Moreover, the activated PAK1 acts as a central node in indispensable oncogenic signaling cascades for the expression of cancer-elicited hallmarks, as it interacts with crucial substrates.[41]

However, designing a highly selective PAK1 inhibitor is quite challenging because of a high homology of the kinase domain and is further hampered by high toxicity, poor potency, poor solubility, isoform specificity, and inadequate testing of existing inhibitors.[41−43] Considering these issues, in this work, a synergistic computational approach was used to repurpose FDA-approved drugs from the DrugBank database against PAK1.[44−47] This synergistic approach includes molecular docking using Glide to understand the binding mode and affinity of the drug molecules revealed through potential noncovalent interaction energies.[48,88] However, the current scoring functions neglect the contributions of protein flexibility and the effects of explicit water molecules at the binding site, which could provide a better estimation of the complex's binding affinity.[49−51]

Therefore, WaterMap (WM) is a tool used to predict the effects of explicit water molecules at the protein binding site.[50] In WaterMap, a short 2 ns MD simulation is performed using the Grand Canonical Monte Carlo (GCMC) sampling to predict structurally weak water clusters in the protein binding pocket. These water clusters are characterized by an unfavorable binding free energy (indicated by a positive $\Delta\Delta G$ for a water molecule that is placed in a region instead of the bulk solvent) and are typically localized at hydrophobic regions of the protein binding site. Since subtle differences in the binding site will result in significant differences in the binding pocket hydration sites, designing or repurposing drug molecules that displace unfavorable water molecules can result in highly selective drug molecules.[52−58] Finally, molecular dynamics simulations were performed in triplicate to test the repurposing of the selected FDA-approved drugs as potential PAK1 inhibitors.[48,59] The best three identified drug molecules

https://doi.org/10.1021/acsomega.1c02032
ACS Omega 2021, 6, 26829−26845

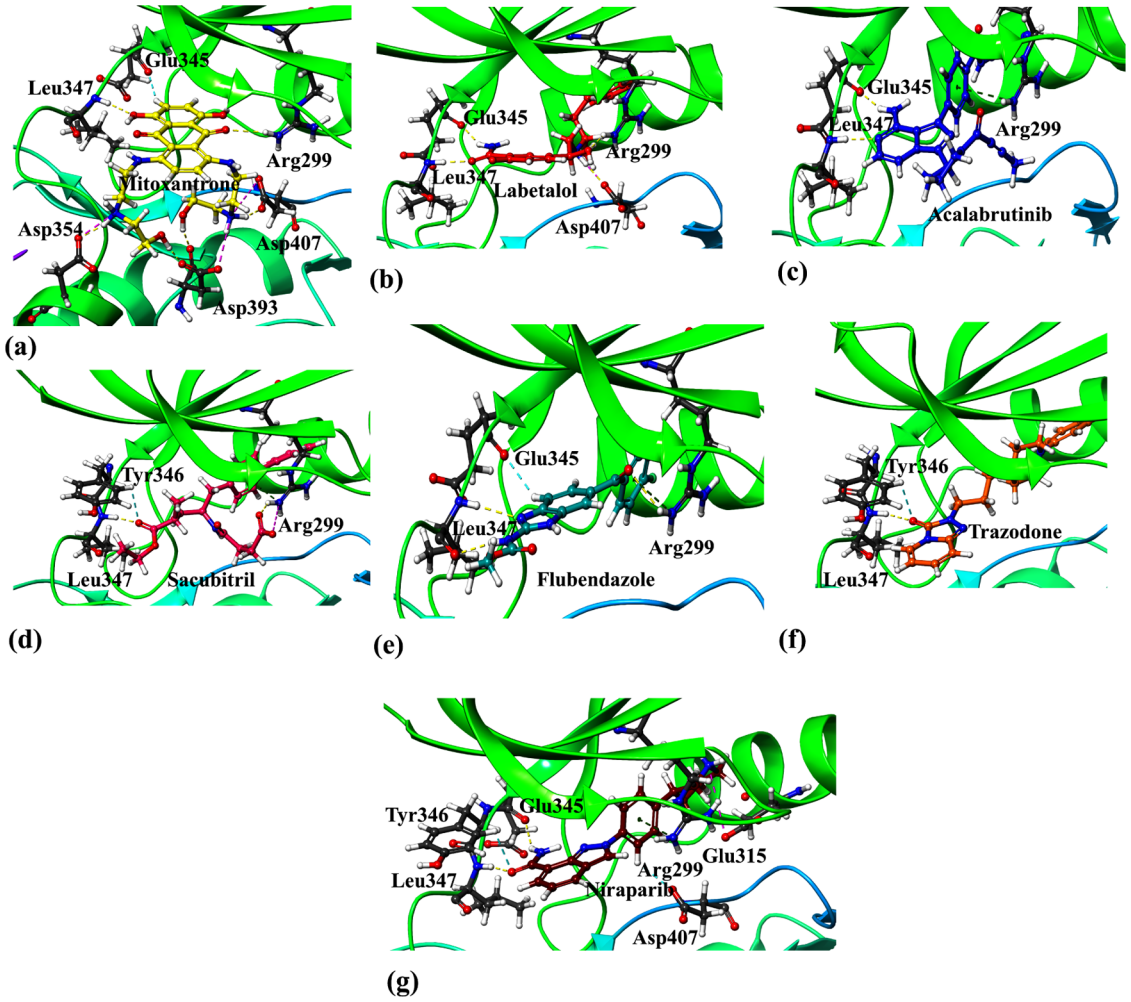

Figure 2. (a–g) Three-dimensional interaction pattern of PAK1 and seven repurposable drug molecules, where yellow dotted lines and blue, green, and magenta colors indicate hydrogen-bond interactions, aromatic hydrogen-bond, cation–π interactions, and salt bridges, respectively.

will be considered for *in vitro* analysis to deduce their potential as promising PAK1 inhibitors.

RESULTS AND DISCUSSION

Identification of Potential PAK1 Repurposable Inhibitors Using Virtual Screening, Hydration Site Thermodynamics, and Molecular Dynamics Simulation Approaches. We adopted a virtual screening workflow to identify PAK1 repurposable inhibitors through the prepared crystal structure of PAK1 (PDB id: 4EQC[37]) and curated FDA-approved drugs from DrugBank database.[47] All of the FDA-approved molecules with validated pharmacokinetic properties and toxicological profiles were docked at the ATP-binding cavity,[37,48,107] (Figure S1) of PAK1 employing the Glide docking program in three different modes, namely, the high-throughput virtual screening (HTVS), standard precision (SP),[60,61] and extra precision (XP).[62] Approximately, 2162 FDA-approved molecules were processed through HTVS docking wherein the top 700 molecules were selected for further screening based on the docking score and interaction pattern, as described later. Then, these 700 molecules were subjected to the next level of filter, that is, the SP mode in which 250 molecules were selected for further screening using XP. From the XP mode of docking, the top 100 molecules were analyzed, of which 27 drug molecules were considered for further calculations, based on the below criteria (Figure 1). These 27 drug molecules displayed hydrogen-bond interactions, hydrophobic contacts, and salt bridges as shown in Figure S3 with the key residues Arg299, Glu345, Leu347, Asp354, Asp393, and Asp407. The glide score for these molecules ranged from −15.792 to −4.525 kcal/mol. The PAK1 amino acid residues Ile276, Glu315, Tyr346, and Thr406 were involved in interactions with the molecules Paromycin, Faramycetin, Pazopanib, Diosmetin, Fluconazole, and Rosiglitazone (Table S1). Besides, the steric, electrostatic, or van der Waals interactions in the protein active site, with additional factors involved in the binding process like the displacement of weakly bound structural water molecules, enhanced the understanding of binding affinity and subsequent potency gains in the selected 27 drug molecules.[63]

Characterizing Hydration Sites toward the Selectivity of Seven PAK1 Repurposable Inhibitors. The WaterMap calculations facilitated the identification of localized hydration sites around the binding cavity of PAK1, with a breakdown of thermodynamic energetic profiles such as enthalpy (ΔH), entropy ($-T\Delta S$), and differential binding energy ($\Delta\Delta G$). From the perspective of drug design that is based on the differential binding energy $\Delta\Delta G$, the overlapping hydration sites on ligand functional groups could be categorized into displaceable ($\Delta\Delta G \gg 0$ and $\Delta H \gg 0$), replaceable ($\Delta H \ll 0$

https://doi.org/10.1021/acsomega.1c02032
ACS Omega 2021, 6, 26829−26845

Table 1. Energy and Interaction Profile of the Shortlisted Seven Drugs as Potential PAK1 Inhibitors

s. no	drug	indication	glide score (kcal/mol)	glide energy (kcal/mol)	interactions (D−H···A)	distance (Å)
1.	Mitoxantrone	antineoplastic	−12.343	−65.039	N^+H_2(Arg299)···O=C	2.62
					C−H···O(Glu345)	2.30
					N−H(Leu347)···O	2.14
					N^+H_2···O^-(Asp354)	1.73
					O−H···O(Asp393)	1.70
					N^+H_2···O(Asp407)	1.75
					N^+H_2(Arg299)···OH	1.88
					NH_2···O=C(Glu345)	1.95
2.	Labetalol	antihypertensive	−9.989	−43.089	C−H(Tyr346)···O	2.50
					N−H(Leu347)···O	1.84
					N^+H_2···O^- (Asp407)	1.80
3.	Acalabrutinib	BTK inhibitor	−9.937	−50.653	NH_2···O=C(Glu345)	1.84
					N−H(Leu347)···N	2.10
					N^+H_2(Arg299)···O	1.91
4.	Sacubitril	prodrug inhibiting neprilysin	−9.363	−51.242	C−H(Tyr346)···O	2.75
					N−H(Leu347)···O	1.86
					N^+H_2(Arg299)···O	2.54
5.	Flubendazole	antihelminitic	−8.457	−43.375	C−H···O(Glu345)	2.61
					N−H(Leu347)···N	2.60
					N−H···O(Leu347)	2.13
6.	Trazodone	antidepressant	−7.908	−49.043	C−H(Tyr346)···O	2.75
					N−H(Leu347)···O	2.02
					NH_2···O=C(Glu345)	2.19
7.	Niraparib	PARP inhibitor	−6.880	−44.874	C−H(Tyr346)···O	2.75
					N−H(Leu347)···O	1.84
					C−H···O^-(Asp407)	2.62

and yet $\Delta\Delta G \gg 0$ or $\cong 0$), and stable ($\Delta\Delta G \ll 0$) water molecules.[64] Relatively, the entropy of a hydration site is always unfavorable near the protein than in bulk solvent.[65] An extensive thermodynamic analysis of hydration sites (HSs) is important for drug design since the displacement of high-energy HSs from the protein binding site is a driving source of binding affinity.[52] The thermodynamic profiles and HS localizations for 27 drug molecules are provided in the Supporting Information, of which 20 drugs molecules are observed to displace a smaller number of high-energy HSs and hence may not offer better selectivity to PAK1 (Figure S4). However, the approved drugs for cancer therapy such as Vandentanib, Ribociclib, Polydatin, and Pazopanib and antibiotics like Paromomycin and Framycetin displaced high-energy HSs with a considerable number of stable and favorable hydration sites (Table S2). Consequently, these drug molecules may possibly lower the binding affinity and potency as PAK1 inhibitors owing to displaced favorable hydration sites.

Therefore, the seven FDA-approved drugs, namely, Mitoxantrone,[66] Labetalol,[67] Acalabrutinib,[68] Sacubitril,[69] Flubendazole,[70] Trazodone,[71] and Niraparib,[72] were scrutinized based on displacing more unfavorable hydration sites,[55,63,73] to consequently improve virtual screening results[63] (Figure 1). From the docking results, we observed that the Mitoxantrone had the highest glide score of −12.243 kcal/mol and showed more hydrogen-bond interactions, hydrophobic contact (cation−π), and salt bridges with Arg299, Glu345, Asp354, Asp393, and Asp407. An aromatic hydrogen-bond interaction was observed with the amino acid residue Tyr346 in Labetalol, Sacubitril, Trazodone, and Niraparib drug molecules. However, the loss of salt bridges and other interactions were witnessed in Acalabrutinib, Sacubitril, Flubendazole, and Trazodone unlike in Labetalol and Niraparib, which showed ionic contacts with residues Glu315 and Asp407. All of the molecules displayed hydrogen-bond interactions and a hydrophobic cation−π contact with Arg299, Glu345, and hinge region amino acid residue Leu347 that were consistent with the pattern observed in PAK1 complex structures (Figure 2a−g) (Figures S2 and S5) (Table 1).[74−77] The molecular docking technique sorted and evaluated the conformation of the selected drug molecules based on their binding efficiency, which indicated some pharmacological activity with PAK1. The seven shortlisted drug molecules were considered for exploring the implications of hydration site displacements in determining the binding affinity gains and their selectivity behavior with PAK1.

The WM results indicate that except Mitoxantrone, all of the other molecules were found positioned toward the hydrophobic cavity of PAK1, and therefore, high-energy unfavorable hydration sites HSs such as 57, 62, 65, 91, and 109 were localized and identified in the mentioned region. However, HSs 80 and 107 located in the drug molecules Mitoxantrone, Sacubitril, and Trazodone had $\Delta\Delta G \gg 0$, which were not as high as the earlier hydration sites. The HS 107 showed favorable $\Delta H < 0$ typical of an enthalpic-driven hydrophobic effect. The HS 21 (ΔH = −0.27 kcal/mol; $-T\Delta S$ = 2.86 kcal/mol and $\Delta\Delta G$ = 2.59 kcal/mol) was overlapped by the chemical moieties of all molecules involved in the hinge region residue Leu347, which described a strong enthalpic interaction with protein. The displaceable HS 103 (ΔH = −0.28 kcal/mol; $-T\Delta S$ = 1.02 kcal/mol; and $\Delta\Delta G$ = 0.74 kcal/mol) identified in the molecules Mitoxantrone, Labetalol, Acalabrutinib, Flubendazole, and Trazodone had similar thermodynamic profile trends as in the HS 21, which represented a water molecule candidate for replacement, by a ligand functional

https://doi.org/10.1021/acsomega.1c02032
ACS Omega 2021, 6, 26829−26845

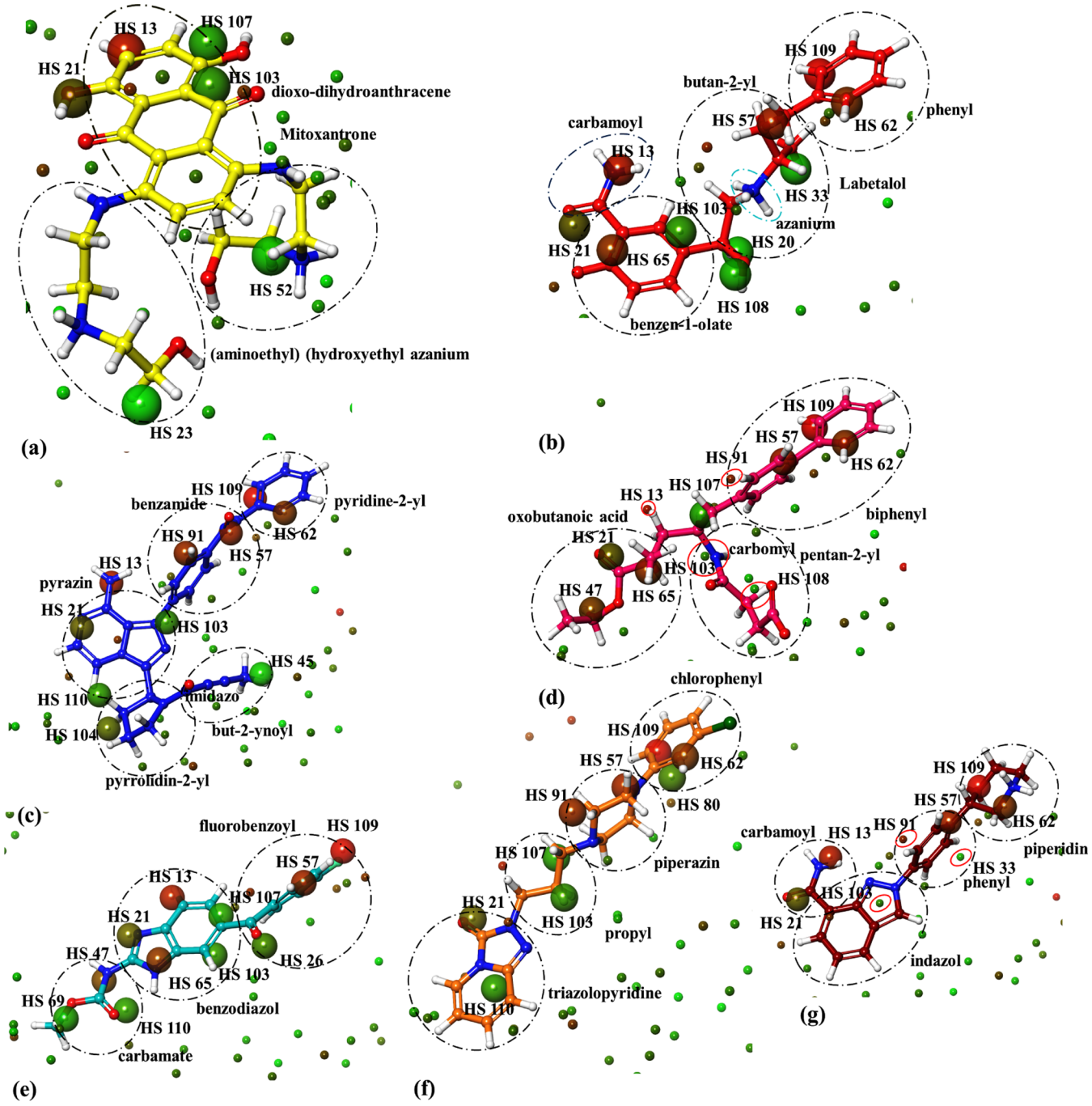

Figure 3. (a–g) Localization of green favorable and red unfavorable hydration sites where black encircled portions represent the chemotypes of seven drug repurposable molecules involved in displacement and red represents the nondisplaced hydration sites.

group that could justify the entropic penalty. Similarly, the HS 110 (in molecules Mitoxantrone, Acalabrutinib, Flubendazole, and Trazodone) showed $\Delta H \cong 0$ and $\Delta\Delta G > 0$, which indicated the enthalpy of bulklike characteristics and displacement of this HS, which could lead to an increase in binding affinity and subsequent potency gains of the drug molecules. The favorable HSs 45 and 69, localized near the chemotype CH, were observed in molecules Acalabrutinib and Flubendazole, respectively, had ΔH, $-T\Delta S$, and $\Delta\Delta G < 0$, indicating that these were stable water molecules and should be avoided for displacement. Comparatively, Mitoxantrone (HSs 23 and 52) and Labetalol (HSs 20, 33, and 108) had many favorable hydration sites, with $\Delta\Delta G < 0$ that were enthalpically driven due to charged–dipole interactions localized at the polarized chemotype NH^+, involved in hydrogen-bond and salt-bridge interactions with ionized residues Asp354 and Asp407. The HS 13 was displaced in all of the molecules except in Sacubitril and Trazodone. This was characterized by a large positive $-T\Delta S$ value (3.33 kcal/mol), suggesting an unfavorable entropic gain. The dislocation of this HS into bulk solvent can rationalize the penalty. We observed that molecules Acalabrutinib, Flubendazole, and Trazodone had thermodynamically greater unfavorable HSs that were displaced, and therefore anticipated stronger binding affinity gains and enhanced selectivity to PAK1 (Figures 3a–g and Table 2).

https://doi.org/10.1021/acsomega.1c02032
ACS Omega 2021, 6, 26829–26845

Table 2. Thermodynamic Properties of Computationally Predicted and Selected Hydration Sites in Drug Molecules Mitoxantrone, Labetalol, Acalabrutinib, Sacubitril, Flubendazole, Trazodone, and Niraparib

	site	occupancy	overlap	ΔH (kcal/mol)	$-T\Delta S$ (kcal/mol)	$\Delta\Delta G$ (kcal/mol)
Mitoxantrone	13	0.89	1.0	1.94	3.33	5.27
	21	0.83	1.0	−0.27	2.86	2.59
	23	0.81	0.79	−4.52	3.02	−1.50
	52	0.60	1.0	−2.74	2.08	−0.66
	103	0.37	1.0	−0.28	1.02	0.74
	107	0.34	1.0	−0.81	1.04	0.23
Labetalol	13	0.89	1.0	1.94	3.33	5.27
	20	0.85	0.0	−3.81	3.04	−0.77
	21	0.83	1.0	−0.27	2.86	2.59
	33	0.74	0.0	−3.23	2.60	−0.63
	57	0.55	0.0	3.14	1.52	4.66
	62	0.52	0.0	2.43	1.50	3.93
	65	0.50	1.0	2.56	1.44	4.00
	103	0.37	1.0	−0.28	1.02	0.74
	108	0.34	1.0	−1.30	1.00	−0.30
	109	0.34	0.0	5.42	1.02	6.44
Acalabrutinib	13	0.89	1.0	1.94	3.33	5.27
	21	0.83	1.0	−0.27	2.86	2.59
	45	0.64	0.31	−3.05	2.07	−0.98
	57	0.55	0.0	3.14	1.52	4.66
	62	0.52	0.0	2.43	1.50	3.93
	91	0.40	0.0	3.14	1.22	4.36
	103	0.37	1.0	−0.28	1.02	0.74
	104	0.36	0.88	1.17	1.07	2.24
	109	0.34	0.0	5.42	1.02	6.44
	110	0.33	1.0	−0.28	0.91	0.63
Sacubitril	21	0.83	1.0	−0.27	2.86	2.59
	47	0.63	0.16	1.50	1.95	3.45
	57	0.55	0.0	3.14	1.52	4.66
	62	0.52	0.0	2.43	1.50	3.93
	65	0.50	1.0	2.56	1.44	4.00
	107	0.34	1.0	−0.81	1.04	0.23
	109	0.34	0.0	5.42	1.02	6.44
Flubendazole	13	0.89	0.44	1.94	3.33	5.27
	21	0.83	1.0	−0.27	2.86	2.59
	26	0.79	0.006	−1.29	2.67	1.38
	47	0.63	1.0	1.50	1.95	3.45
	57	0.55	1.0	3.14	1.52	4.66
	65	0.50	1.0	2.56	1.44	4.00
	69	0.49	0.04	−1.46	1.42	−0.04
	103	0.37	1.0	−0.28	1.02	0.74
	107	0.34	1.0	−0.81	1.04	0.23
	109	0.34	1.0	5.42	1.02	6.44
	110	0.33	0.22	−0.28	0.91	0.63
Flubendazole	13	0.89	0.44	1.94	3.33	5.27
	21	0.83	1.0	−0.27	2.86	2.59
	26	0.79	0.06	−1.29	2.67	1.38
	47	0.63	1.0	1.50	1.95	3.45
	57	0.55	1.0	3.14	1.52	4.66
	65	0.50	1.0	2.56	1.44	4.00
	69	0.49	0.04	−1.46	1.42	−0.04
	103	0.37	1.0	−0.28	1.02	0.74
	107	0.34	1.0	−0.81	1.04	0.23
	109	0.34	1.0	5.42	1.02	6.44
	110	0.33	0.22	−0.28	0.91	0.63
Trazodone	110	0.33	0.22	−0.28	0.91	0.63
	57	0.55	1.0	3.14	1.52	4.66
	62	0.52	1.0	2.43	1.50	3.93
	80	0.44	1.0	0.03	1.40	1.43
	91	0.40	0.89	3.14	1.22	4.36

https://doi.org/10.1021/acsomega.1c02032
ACS Omega 2021, 6, 26829−26845

Table 2. continued

	site	occupancy	overlap	ΔH (kcal/mol)	$-T\Delta S$ (kcal/mol)	$\Delta\Delta G$ (kcal/mol)
	103	0.37	1.0	-0.28	1.02	0.74
	107	0.34	1.0	-0.81	1.04	0.23
	109	0.34	1.0	5.42	1.02	6.44
	110	0.33	1.0	-0.28	0.91	0.63
Niraparib	13	0.89	1.0	1.94	3.33	5.27
	21	0.83	1.0	−0.27	2.86	2.59
	57	0.55	0.0	3.14	1.52	4.66
	62	0.52	1.0	2.43	1.50	3.93
	109	0.34	1.0	5.42	1.02	6.44

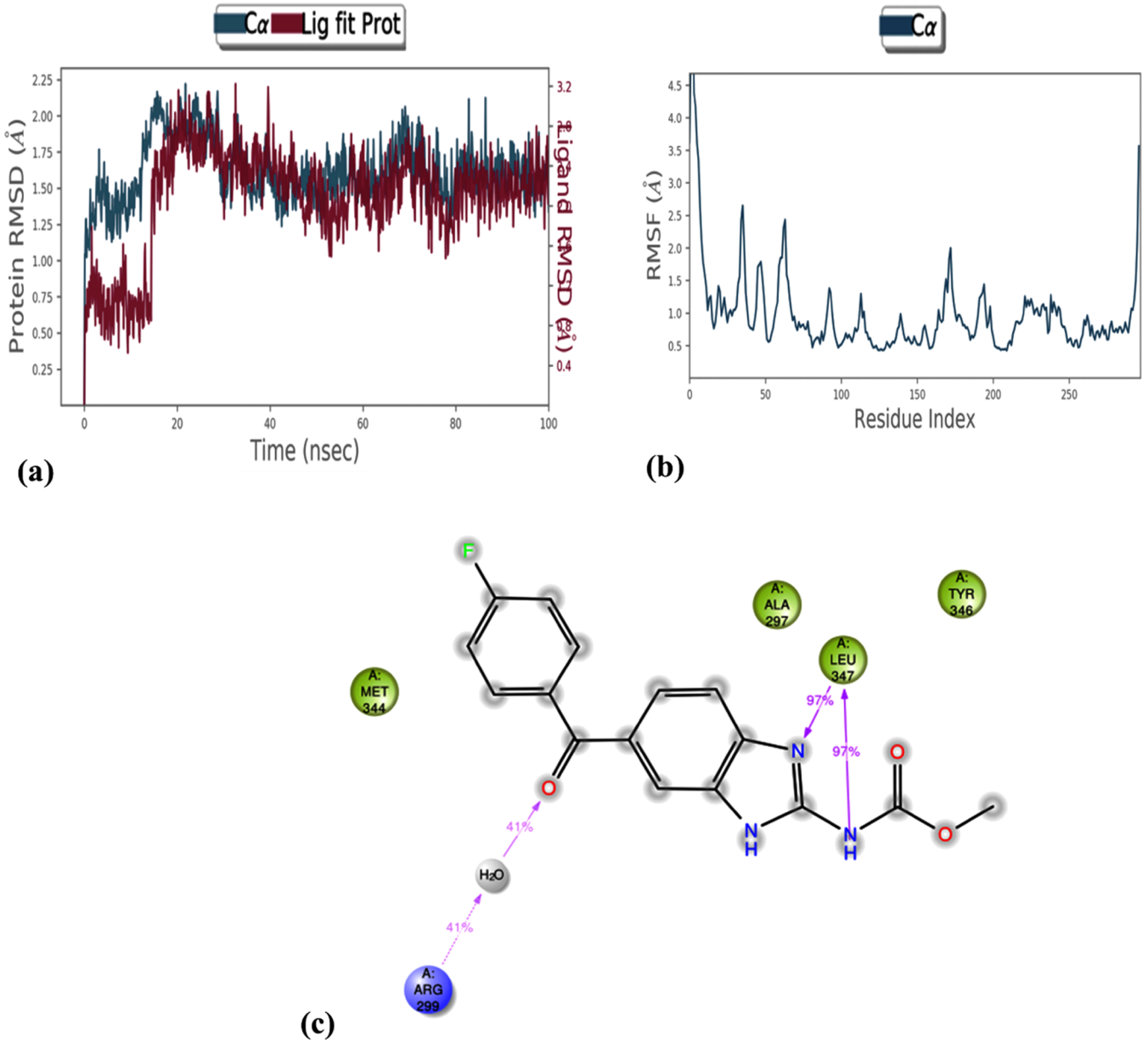

Figure 4. (a) Root-mean-square deviation (RMSD), (b) root-mean-square fluctuation (RMSF), and (c) intermolecular interactions between PAK1 and Flubendazole.

Stability Analysis of Selected Seven Drug Molecules Using Molecular Dynamics (MD) Simulations. The seven molecules selected after WaterMap calculations were considered for molecular dynamics (MD) simulations. We performed three independent simulations for each complex, for 100 ns each, to ensure that results were not biased to the starting seed. Then, the trajectory of each complex for each run was analyzed using metrics such as root-mean-square deviation (RMSD), root-mean-square fluctuation (RMSF), and intermolecular interactions to quantify the structural changes. The RMSD

https://doi.org/10.1021/acsomega.1c02032
ACS Omega 2021, 6, 26829−26845

Table 3. Average RMSD Values of Seven Drug Repurposable Molecules Obtained from MDS Performed in Triplicate

		RUN1		RUN2		RUN3		average RMSD (Å)	
s. no	drugs	PAK1	ligand	PAK1	ligand	PAK1	ligand	PAK1	ligand
1.	Niraparib	3.03 ± 0.50	2.55 ± 0.64	1.86 ± 0.22	1.55 ± 0.49	1.61 ± 0.16	2.12 ± 0.37	2.16	2.07
2.	Trazodone	1.85 ± 0.27	2.52 ± 0.39	2.03 ± 0.33	2.70 ± 0.58	2.52 ± 0.46	3.39 ± 0.88	2.13	2.87
3.	Flubendazole	1.71 ± 0.27	2.31 ± 0.42	1.87 ± 0.18	1.72 ± 0.30	1.61 ± 0.17	1.53 ± 0.34	1.73	1.85
4.	Mitoxantrone	2.13 ± 0.31	4.23 ± 1.17	1.76 ± 0.28	4.00 ± 0.57	1.65 ± 0.17	4.04 ± 0.74	1.84	4.09
5.	Labetalol	2.99 ± 0.47	8.74 ± 2.14	2.36 ± 0.44	2.10 ± 0.59	1.86 ± 0.34	6.28 ± 2.65	2.40	5.70
6.	Acalabrutinib	2.11 ± 0.28	3.04 ± 1.00	1.67 ± 0.23	3.36 ± 0.62	1.66 ± 0.19	1.81 ± 0.61	1.81	2.73
7.	Sacubitril	2.14 ± 0.42	4.80 ± 1.68	3.12 ± 0.58	3.42 ± 1.08	2.20 ± 0.37	3.07 ± 0.80	2.48	3.56

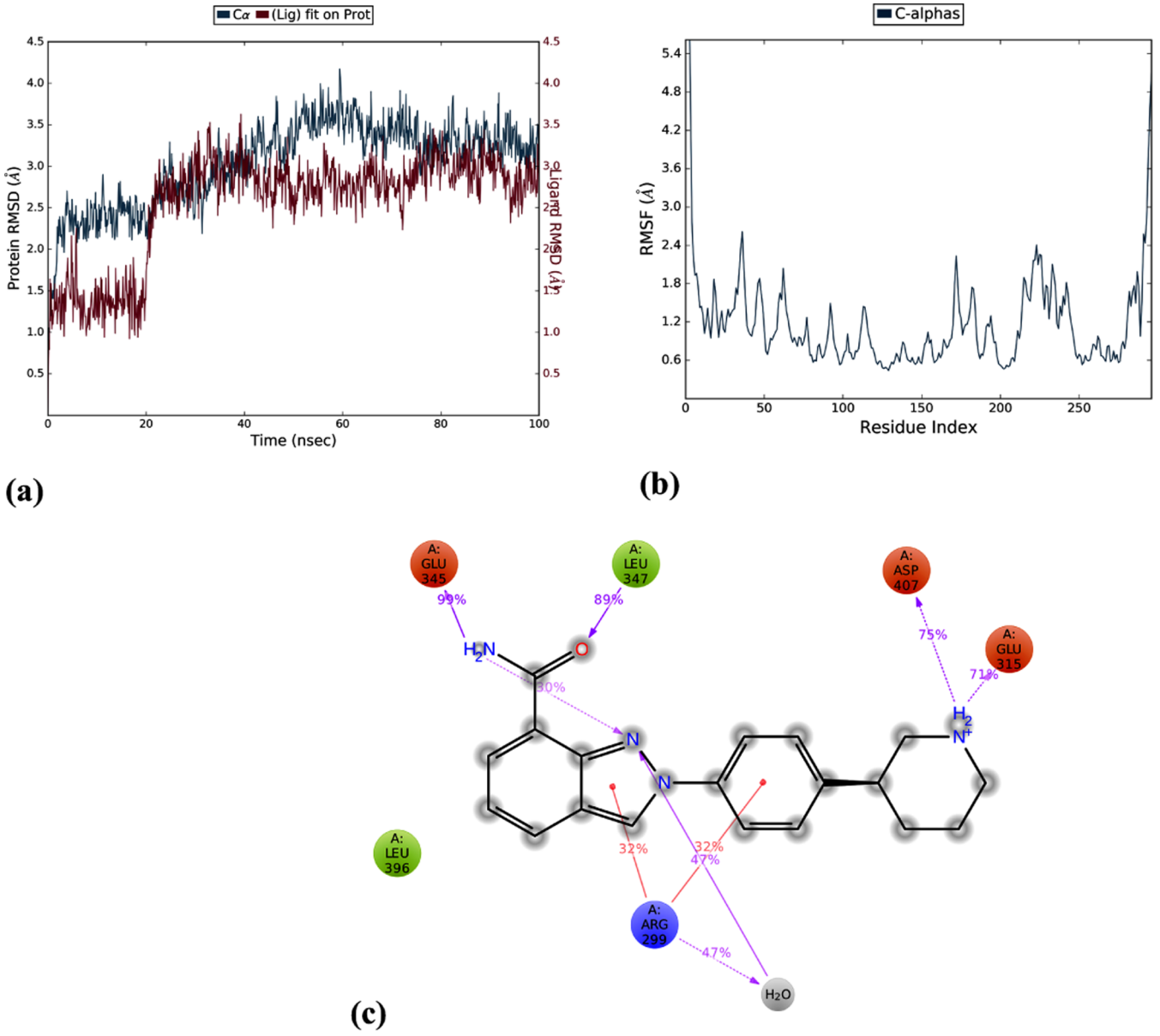

Figure 5. (a) Root-mean-square deviation (RMSD), (b) root-mean-square fluctuation (RMSF), and (c) intermolecular interactions between PAK1 and Niraparib.

plot corresponding to the protein backbone for seven PAK1–drug complexes, including its average values, are given in Figures 4–6 and Table 3. The Cα of PAK1 protein showed no major structural deviations with an average RMSD ranging between 1.8 and 2.5 Å, indicating its reproducible stability in all runs, for each drug complex. However, Mitoxantrone, Labetalol, and Sacubitril displayed high average RMSDs of 4.09, 5.70, and 3.56 Å, respectively, from the initial docked poses, indicating that these drug molecules were not firmly held in the binding pocket due to loss of crucial interactions that are responsible for the stability of the overall systems. Flubendazole (Figure 4a) was highly stable, followed by

https://doi.org/10.1021/acsomega.1c02032
ACS Omega 2021, 6, 26829–26845

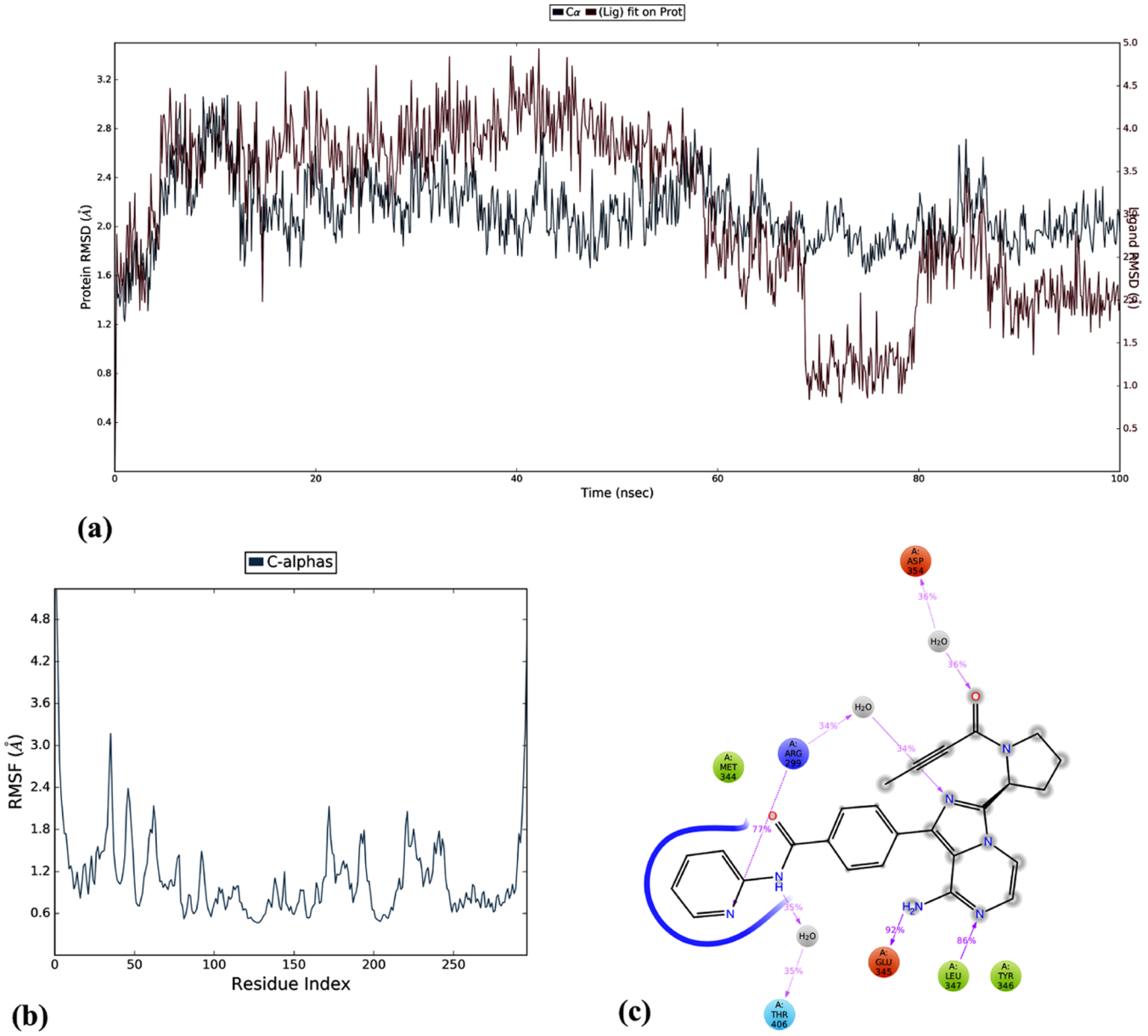

Figure 6. (a) Root-mean-square deviation (RMSD), (b) root-mean-square fluctuation (RMSF), and (c) intermolecular interactions between PAK1 and Acalabrutinib.

Niraparib (Figure 5a), Acalabrutinib (Figure 6a), and Trazodone drug molecules, as given in Table 3. The RMSF of the PAK1 protein in complex with seven drug molecules and the active site residues of the binding pocket are listed in Table S3. This revealed that the increased per-residue fluctuations were higher in the N-lobe than the C-lobe of the kinase domain, due to its flexible loop regions that contributed to its high mobility.[37,107]

In the case of PAK1-Mitoxantrone, the interaction pattern displayed a loss of interactions with Arg299 and Asp407 in replicates 2 and 3, with an enhanced interaction to Asp407 that behaved like a short-lived contact in replicate 1 (Figures S15c and S22c). Similarly, Arg299 also showed no interactions in all of the MD triplicate of PAK1−Labetalol (Figures S9c, S16c, and S23c). However, Leu347 was observed as a hydrogen-bond interaction for more than 50% of the simulation time in replicates 2 and 3 (Figures S16c and S23c), which was negligible in replicate 1 (Figure S9c). Besides, loss of interactions such as Lys308 and Glu315 was perceived in replicates 2 and 3 (Figures S16c and S23c) and the Asp407 interaction was prominently retained in all of the three replicates of the PAK1−Labetalol complex (Figures S9c, S16c, and S23c). In the PAK1−Acalabrutinib complex, interactions with crucial amino acid residues Arg299, Glu345, and Leu347 including the vital hydrophobic interactions were present in all of the three replicates contributing to the stability of the complex (Figures 6c, S12c, and S19c). Likewise, most of the interaction fractions in the PAK1−Sacubitril complex were maintained (Figures S7c, S14c, and S21c). However, in replicate 3, the hydrophobic contacts (Val342 and Met344) and the hydrogen-bond interactions with Leu347 and Lys538 were diminished with the water-mediated contacts (Figure S21c). Nevertheless, the molecular interactive forces like the hydrogen-bond interaction with Leu347 and hydrophobic contacts involving Ala297, Met344, Tyr346, and Leu396 were present for <75% of the simulation time and stable in all of the

https://doi.org/10.1021/acsomega.1c02032
ACS Omega 2021, 6, 26829−26845

three replicates of the PAK1−Flubendazole complex (Figures 4c, S10c, and S17c). In the PAK1−Niraparib complex, the interactions with crucial amino acid residues Glu315, Glu345, and Leu347 were maintained in all of the three replicates (Figures 5c, S11c, and S18c). Also, apparent loss of hydrophobic contacts with Arg299 and Leu396, including a hydrogen-bond interaction with Asp407, were observed. Additionally, hydrophobic contacts with amino acid residues such as Tyr330, Val342, and Met344 were formed in replicates 2 and 3 (Figures S11c and S18c). As observed in the PAK1−Acalabrutinib complex, the PAK1−Trazodone complex showed a similar prominent interaction pattern in replicate 3 (Figure S13c) as observed in replicate 1 (Figure S6c). The ligand average RMSD of 2.87 Å was due to the loss of crucial interaction with Leu347 in replicate 2 (Figure S20c). The MD simulation analyses suggested that the PAK1 complexed with molecules Flubendazole, Niraparib, and Acalabrutinib were highly stable in terms of structural stability and the occurrence of consistent interactions throughout the simulation time (in triplicates) as shown in Tables 3 and 4.

Table 4. Qualitative Categorical Classification of Seven FDA-Approved Molecules[a]

s. no	molecules	MDS	WM	docking
1.	Flubendazole	+++++	+++++	+++
2.	Niraparib	+++++	+++	+
3.	Acalabrutinib	+++++	+++++	+++++
4.	Trazodone	++++	+++++	++
5.	Mitoxantrone	+++	++	+++++
6.	Sacubitril	++	++++	++++
7.	Labetalol	+	+++	+++++

[a]+++++ denotes the best three molecules based on RMSD and interaction fractions (MDS); higher number of displaced unfavorable hydration sites (WM) and energy score and interaction profiles (Docking).

Analysis of Frontier Molecular Orbitals. The frontier molecular orbital energies (highest occupied molecular orbital (HOMO) and lowest unoccupied molecular orbital (LUMO)) were calculated for seven drug molecules Mitoxantrone, Labetalol, Acalabrutinib, Sacubitril, Flubendazole, Trazodone, and Niraparib obtained from the DrugBank database and selected based on the docking score, interaction pattern, and displacement of unfavorable hydration sites. The molecules were geometrically optimized at the B3LYP/6-31G** level. The generated HOMO and LUMO maps are shown in Figure 7 and Table 5, where the blue- and red-colored portions represent the electron cloud density of FMOs to donate (HOMO; nucleophilic attack) and accept (LUMO; electrophilic attack) electrons from atoms engaged in chemical reaction.[78] The HOMO and LUMO values for seven molecules ranged from −0.196 to −0.239 eV and from −0.039 to −0.105 eV, respectively. Besides the HOMO−LUMO energy distribution, the energy gap (HLG) was calculated as a measure of chemical stability, reactivity, and lowest excitation energy of the molecule. These were deduced through electron transfer between the energy levels. Accordingly, the energy gap of the molecules varied between 0.09 and 0.2 eV, of which the low energy gap value suggested better stability and less reactivity of the molecules.[79]

The HOMO electron densities in the drug molecule Mitoxantrone were observed at the chemotype NH of chemical moiety phenyl. This had bi-extensions of (2-aminoethyl) (2-hydroxyethyl) azanium involved in hydrogen-bond and salt-bridge interactions with Asp354, Asp393, and Asp407 (Figure 7a). However, the LUMO was localized at the π-ring systems, namely, dioxo-dihydroanthracen-1-yl and phenyl, where the earlier fused ring accepted electrons from the positively charged guanidium group of Arg299 and NH atom of Leu347. Subsequently, in Labetalol, the HOMO orbitals were distinctively placed at the benzene-1-olate and partially on the O^- of the same chemical moiety. Likewise, the chemical moiety carbamoyl donated and accepted electrons from the amino acid residues Glu345 and Leu347 and hence, the LUMO was majorly positioned with the chemical moiety benzene-1-olate (Figure 7b). For the Acalabrutinib molecule, the HOMO orbitals were located at NH_2; N of fused ring moiety imidazo and pyrazin that acted as electron acceptor and donor with amino acid residues Glu345 (C═O) and Leu347 (NH). The LUMO were mapped in the chemical moieties pyridine and benzamide rings, where the earlier aromatic system involved in the cation−π interaction with Arg299 depicted the chemical reactivity of the molecule (Figure 7c). The molecule Sacubitril demonstrated that the HOMO was delocalized mainly over the chemical group propanoate (O^-), which was involved in cation−π and salt-bridge interactions with positively charged guanidino group of Arg299. The LUMO was located at biphenyl rings where one of the phenyl rings formed a cation−π interaction with Arg299 (Figure 7d). The molecule Flubendazole illustrated the presence of HOMO delocalization particularly in NH chemotype of the chemical group benzodiazol as well as the formation of hydrogen-bond interactions with the hinge region residue Leu347. Meanwhile, the LUMO was mainly located at the oxygen atom and partially in the chemical group fluorobenzoyl, which formed hydrogen-bond and cation−π interactions with Arg299 (Figure 7e). Also, in the Trazodone molecule, HOMO orbitals were located at C and N chemotypes of the aromatic rings chlorophenyl and piperazin, whereas the LUMO orbitals were located at triazolopyridine, accepting electrons from NH of Leu347 (Figure 7f). Finally, in the molecule Niraparib, large HOMO and LUMO densities were mapped onto the chemical moiety indazol extending to carbamoyl group, which accepted electrons from the NH group of Leu347 and donated electrons to Glu345. This indicated the reactive nature of the chemical groups involved in chemical reaction (Figure 7g).

According to energy gap values, the drug molecule Mitoxantrone had the least HLG of 0.095 eV, indicating very high chemical stability and feasible polarization, followed by molecules Flubendazole (0.133 eV), Sacubitril (0.150 eV), Trazodone (0.150 eV), Niraparib (0.157 eV), Acalabrutinib (0.177 eV), and Labetalol (0.200 eV), demonstrating an impact on the inhibitory reaction potential against PAK1.

Molecular Electrostatic Surface Potential (ESP) Analysis. The electrostatic surface potential (ESP) maps computed for PAK1 binding pocket, and the final seven drug molecules (Figure S24a) helped us understand the complementarity of protein−ligand interactions. The binding pocket of PAK1 comprises amino acid residues such as Arg299, Glu315, Glu345, Leu347, Asp354, Asp393, and Asp407. Based on the generated color-coded ESP map, blue refers to the electropositive potential enclosed by Arg299, and red denotes the electronegative region, which are defined by Glu315, Glu345, Asp354, Asp393, and Asp407. The ESP indicates that the active site of PAK1 is predominantly surrounded by negatively

https://doi.org/10.1021/acsomega.1c02032
ACS Omega 2021, 6, 26829−26845

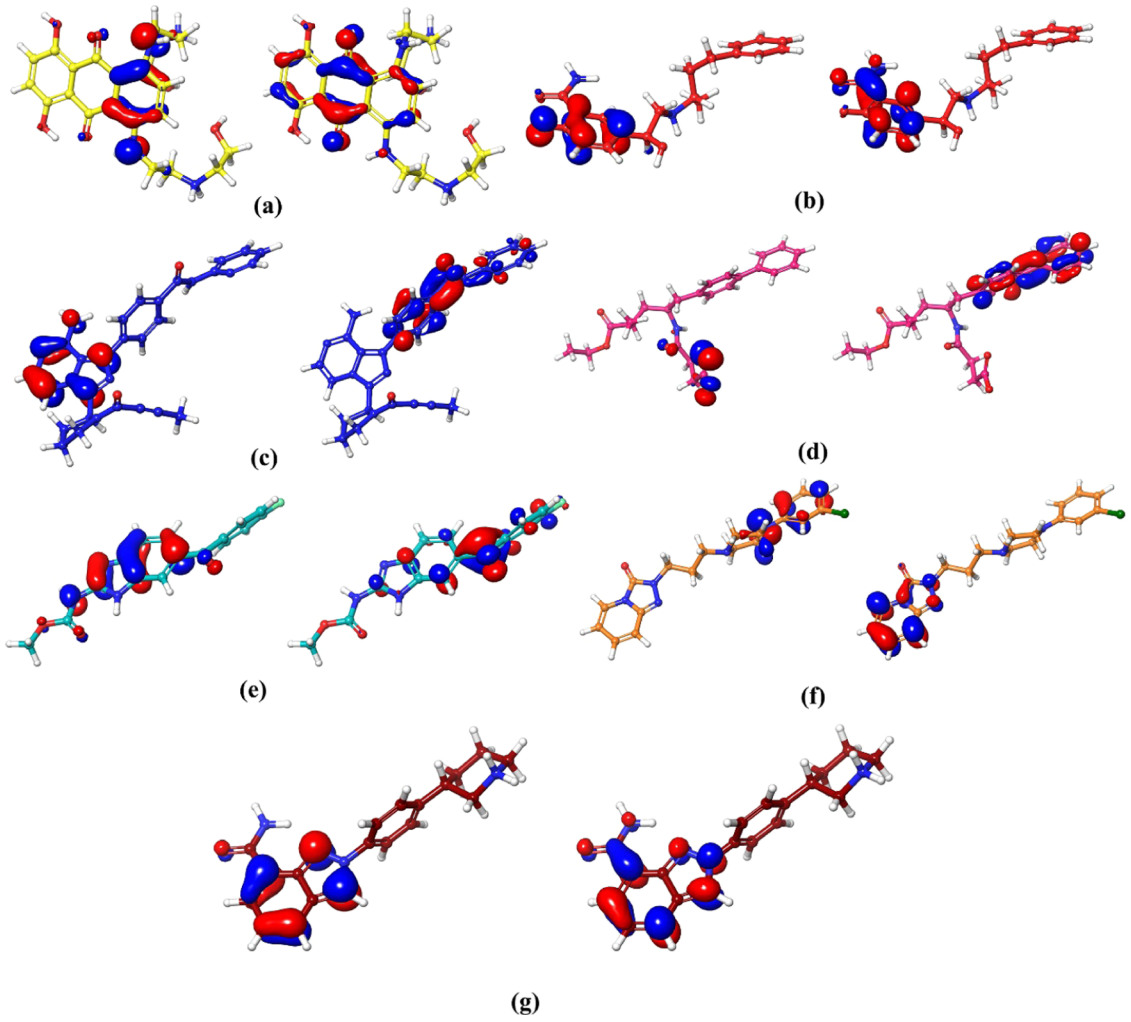

Figure 7. Illustration of localization of HOMO and LUMO orbitals in (a) Mitoxantrone, (b) Labetalol, (c) Acalabrutinib, (d) Sacubitril, (e) Flubendazole, (f) Trazodone, and (g) Niraparib.

Table 5. Frontier Molecular Orbital Energies of Shortlisted Seven Drugs

s. no	drug	HOMO (eV)	LUMO (eV)	HLG (eV)
1.	Mitoxantrone	−0.200	−0.105	0.095
2.	Flubendazole	−0.238	−0.105	0.133
3.	Sacubitril	−0.196	−0.046	0.150
4.	Trazodone	−0.196	−0.046	0.150
5.	Niraparib	−0.220	−0.063	0.157
6.	Acalabrutinib	−0.233	−0.056	0.177
7.	Labetalol	−0.239	−0.039	0.200

charged residues. As shown in Figure S24c, the drug molecules Flubendazole, Niraparib, Acalabrutinib, and Trazodone have better binding affinity due to their preferential binding mode in the hydrophobic region of PAK1 formed by Ile276, Val284, Ala297, Ile316, Met319, Val328, Val342, Met344, Tyr346, Ala348, and Leu396 as seen from the co-crystal ligand FRAX597 (Figure S24b). In particular, the NH^+ extensions of the drug molecule Mitoxantrone are bound toward the electronegative region of PAK1, away from the hydrophobic pocket depicts strong complementarity potentials. Similarly, the MESP maps computed using Schrödinger depict the pronounced electrostatic potentials in the drug molecules (Figure S24d), of which the N^+/NH chemotypes in chemical moieties aminoethyl (Mitoxantrone), azanium/acetamide (Labetalol), imidazopyrazin (Acalabrutinib), carbamate group (Flubendazole), and piperidin (Niraparib) depicted a tendency of donating electrons to amino acid residues Glu315, Glu345, Leu347, Asp354, Asp393, and Asp407, which are either involved in hydrogen-bond or salt-bridge interactions. Likewise, the electronegative potential was mostly characterized by the ionized O^-/OH/O atoms located in chemical moieties dihydroanthracene (Mitoxantrone), but-2-ynoyl/acetamide (Labetalol), oxobutanoic acid/propanoate (Sacubitril), fluorobenzoyl (Flubendazole), triazolopyridine (Trazodone), and carbamoyl group (Niraparib) acted as an electron acceptor from amino acid residues Arg299 and Leu347. Also, certain N atom types exhibited the electronegative character in the chemical groups benzodiazole and imidazopyrazin of drug molecules Flubendazole, and Acalabrutinib respectively. Thus, the MESP maps showed that the final seven drug molecules exhibited the consequential complementarity potentials to the ESP-characterized binding cavity of PAK1.

CONCLUSIONS

PAK1 is a well-characterized therapeutic target that plays a central role in the regulation of cytoskeletal dynamics, motility, and survival. Previous studies highlighted the upregulated PAK1 expression in cancer, brain disorders, viral infections,

https://doi.org/10.1021/acsomega.1c02032
ACS Omega 2021, 6, 26829−26845

and allergies. However, the discovery of the potent and specific PAK1 inhibitor with isoform selectivity is limited. Therefore, ∼2162 FDA-approved drugs housed in the DrugBank database were considered for SBVS to screen selective and nontoxic PAK1 inhibitors. The methodologies involved in this study, like molecular docking, facilitated the identification of PAK1 potent binders well, based on docking score and interaction pattern. Its scoring functions neglect two major aspects about the receptor flexibility and explicit water molecule effects at the binding site. To obtain accurate results in terms of potency and selectivity, WaterMap (WM) and molecular dynamics (MD) simulations were performed to enhance the understanding of the overall binding affinity and subsequent potency gains of the drug molecules. Therefore, in contrast to hierarchical filters *via* scoring functions and favorable interaction patterns, 27 molecules were shortlisted for WaterMap analysis. The WM approach projected additive effects originating due to "displaceable" high-energy hydration sites HSs 13, 21, 47, 57, 62, 65, 91, 104, and 109, to scrutinize the seven molecules Mitoxantrone, Labetalol, Acalabrutinib, Flubendazole, Sacubitril, Trazodone, and Niraparib for MDS. The MD simulated RMSD, RMSF, and interaction profiles in triplicate were analyzed and showed that PAK1 in complex with Flubendazole followed by Niraparib and Acalabrutinib were more stable than other molecules. The high stability of the PAK1−Flubendazole complex was characterized by the stability of the hydrogen bond with Leu347 and hydrophobic interactions with Ala297, Met344, Tyr346, and Leu396. The PAK1−Niraparib complex showed hydrogen-bond interactions with Glu315, Glu345, Leu347, and Asp407, which persisted in all three replicates. Similarly, in the PAK1−Acalabrutinib complex, the stability was attributed to several hydrophobic interactions besides the hydrogen-bond interactions with Arg299, Glu345, and Leu347. Further, the DFT and ESP analyses revealed that the drug molecules were characterized by their chemical properties, which were stable, less reactive, and showed complementary electrostatic potentials. In particular, the drug molecules Flubendazole, Niraparib, and Acalabrutinib had better binding affinity, and this is the first study to describe them as PAK1 repurposable drug candidates using combined virtual screening with rationalized insights from displaced unfavorable hydration sites and stability of the complexes through robust *in silico* approaches.

MATERIAL AND METHODS

Protein and Grid Preparation. The crystal structure of PAK1 kinase domain in complex with FRAX597 inhibitor (PDB id: 4EQC[74,80]) with a resolution of 2.01 Å was considered for this study. This crystal structure contains a mutation at Lys299 to Arg299 and depicts an intermediate state of enzymatic activity reminiscent of the crucial interaction patterns.[37] Before docking, the protein structure for SBVS, was prepared using the protein preparation wizard embedded in the Schrödinger suite,[81] to remove deformed crystallographic artifacts. The protein structure was preprocessed through assigned bond orders, adding hydrogens, detecting disulfide bonds, and adding the missing loops and side chains. Water molecules beyond a cutoff distance of 5 Å were removed.[82] The included hydrogens in the protein structure were optimized with PROPKA at pH and minimized using the force field OPLS3e to their possible natural biological state.[83,84] The binding site of the PAK1 crystal structure was defined by the co-crystallized ligand coordinates,[74] to generate a docking grid for the prepared protein in the grid generation panel with default options. The nonpolar parts of the receptor atoms were scaled by a van der Waal radius of 0.8 Å, with an absolute partial charge cutoff of 0.25 Å to soften interactions between the ligand and the protein structure.[48,53,85]

Ligand Preparation. This study entails a drug repurposing approach to expedite the identification of the potential PAK1 inhibitors from the existing approved drugs, which have extensive information on clinical history and toxicology. Therefore, ∼2162 FDA-approved drugs from the DrugBank database were retrieved and the chemical structures were prepared with the LigPrep module with default settings,[86] for the hierarchical screening procedure. The ligand preparation included optimization at pH 7 ± 2, retention of stereoisomers, assignment of protonation and ionization states, and minimization of structures using OPLS3e force field with implicit solvation settings.[87]

Structure-Based Repurposing of FDA-Approved Drugs *via* Virtual Screening. The virtual screening process of the curated DrugBank FDA-approved molecular structures against PAK1 was performed using GLIDE molecular docking software in Schrödinger suite.[88] The generated grid for the PAK1 protein was used for the stratified docking process. The workflow of molecular docking involved an initial screening of ∼2162 molecules in the high-throughput virtual screening (HTVS[60,89]) mode that employs a restricted conformational sampling to fasten the docking process, and hence, this was considered to bind molecules at the lowest docking precision. Subsequently, at the end of the docking process, the top ∼30% was taken for the next hierarchical filter through a standard precision (SP) mode that extensively performed a conformational space search for the molecules obtained from the HTVS level of docking. Approximately 35% of molecules from SP docking (250 molecules) were chosen to the next level of extra precision (XP)-based screening of molecules, which facilitated the selection of top 40% for further analysis. Based on the criteria mentioned in the Results and Discussion section, the top 27 molecules were selected (Figure 1). The default settings were maintained in all of the three docking stages of the virtual screening process.

WaterMap Calculations. Considering the limitations in molecular modeling methods of protein−ligand binding,[49,53] methods such as WaterMap (WM) implement a molecular dynamics simulation and solvent clustering coupled with statistical thermodynamic analysis to study the role of structure and thermodynamics of binding site water molecules in molecular recognition,[20,90,91] virtual screening enrichments,[91] rationalize structure−activity relationship (SAR),[63,92,93] characterization of potency gains,[55] and selectivity.[55] This procedure involves the determination of quasi-localized positions and quantitative estimation of thermodynamic properties such as enthalpy (ΔH), entropy ($-T\Delta S$), and differential binding energy ($\Delta\Delta G$) for each water molecule based on the inhomogeneous solvation theory.[50,94] For every hydration site, the enthalpy was computed as an average nonbonded energy with the protein and those in bulk water. The excess entropy was generated by numerically integrating the first-order expansion term of spatial and orientation correlation functions. The ligand binding and unbinding events are correlated with gains or losses in ΔH and $-T\Delta S$, eventually determining the equilibrated state of $\Delta\Delta G$ in water molecules.[95] In this study, the crystal structure of PAK1 (PDB id: 4EQC[48,53]) used in our earlier studies was

https://doi.org/10.1021/acsomega.1c02032
ACS Omega 2021, 6, 26829−26845

considered for performing WM calculations and showed that this method could describe the binding affinity and selectivity that bring about potency gains for the selected FDA drug molecules, which was otherwise difficult to explain using traditional techniques.

Density Functional Theory (DFT) and Molecular Electrostatic Potential (MESP) Calculations. The selected seven drug molecules were prepared and minimized using LigPrep for the generation of low-energy three-dimensional (3D) structures. The recognized conformers were further considered for density functional theory (DFT) calculations to understand the molecular electronic features like electron density, electrostatic map, and frontier molecular orbitals (FMOs), which help to elucidate the biological activity, binding affinity, and chemical reactivity of the molecules with PAK1. All DFT calculations were performed using the Jaguar version 9.8 in Schrödinger suite.[96] The complete geometry optimization of the molecular structures was carried out using a hybrid DFT with Becke's three-parameter exchange potential and the Lee−Yang−Parr correlation functional (B3LYP) at the 6-31G** basic set level.[97,98] To simulate under physiological conditions, energy calculations were performed using the Poisson Boltzmann solver in gaseous phase.[99] The electrostatic potential surface (ESP) maps for PAK1 in complex with selected seven molecules were generated using Adaptive Poisson Boltzmann Solver (APBS[100−102]) program in PyMOL for evaluating the electrostatic interactions and the visualization of potential energy surfaces by applying the potential at the solvent accessible surface for colors and charge densities on protein surfaces. Finally, the MESP iso-energy contours were generated at 30 kcal/mol using Schrödinger software.

Molecular Dynamics Simulation (MDS) Studies. The MD simulations of the selected molecules were performed for 100 ns to explain the conformational variability and stability of the complexes, using the Desmond package in the Schrödinger suite.[103] The seven drug molecules with the protein PAK1 were prepared with the refinement of amino acid interactions using the OPLS3e force field. Meanwhile, the protein was solvated in an orthorhombic water box using the simple point charge (SPC) water molecules. The system was neutralized by adding Na^+ counterions. The box size was set in a way that it covers the protein and ligand completely. Also, the system was minimized and equilibrated through the default protocol available in the Desmond package in Schrödinger.[104] SETTLE algorithm was used to constrain the geometry of all covalent bonds containing water molecules.[105] Electrostatic interactions (long-range) were calculated by the particle-mesh Ewald method.[106] After minimizing and equilibrating the solvated protein−ligand system, a temperature relaxation at 300 K, and 1 bar pressure for 24 ps in NPT ensemble, the final MDS run was performed in triplicate (using different initial seeds for assigning velocities) for 100 ns to investigate the stability of the complex through RMSD, RMSF, and other profiles, which were analyzed through the Simulation Interaction Diagram as used previously.[53]

■ ASSOCIATED CONTENT

Supporting Information

The Supporting Information is available free of charge at https://pubs.acs.org/doi/10.1021/acsomega.1c02032.

Illustration of general binding pocket of PAK1 in complex with ATP, available inhibitor complexes to validate the docking of seven drug repurposable molecules (Figures S1 and S2); docking poses corresponding to 27 FDA drugs obtained from XP binding mode (Figure S3 and Table S1); two-dimensional schematic ligand representations of 20 FDA drug molecules obtained from WaterMap calculations is found incompliant owing to smaller number of displaced unfavorable hydration sites (Figure S4); thermodynamics properties of predicted hydration sites in 20 FDA drug molecules (Table S2); two-dimensional schematic ligand representations of PAK1 with selected seven FDA drugs obtained in XP binding mode, which were selected based on hinge region interactions with unfavorable hydration site displacements besides docking score (Figure S5); RMSF values of PAK1 active site residues in seven drug repurposable molecules obtained from (MD) simulation performed in triplicate (Table S3); root-mean-square deviation (RMSD), root-mean-square fluctuation (RMSF), and intermolecular interactions between PAK1 and seven repurposable drug molecules in triplicate; detailed interpretation of docking, hydration site, and simulation interaction results of PAK1 (first replica) and the seven repurposable drug molecules (Figures S6−S23); and electrostatic potentials of PAK1's binding cavity with final seven drug molecules and their prediction of ionizable regions through MESP maps (Figure S24) (PDF)

■ AUTHOR INFORMATION

Corresponding Author

Jeyakanthan Jeyaraman − *Structural Biology and Bio-Computing Laboratory, Department of Bioinformatics, Science Block, Alagappa University, Karaikudi 630 004 Tamil Nadu, India;* orcid.org/0000-0002-4594-9610; Phone: +91 4565 230725; Email: jjkanthan@gmail.com, jjeyakanthan@alagappauniversity.ac.in; Fax: +91 4565 225202

Authors

Jayashree Biswal − *Structural Biology and Bio-Computing Laboratory, Department of Bioinformatics, Science Block, Alagappa University, Karaikudi 630 004 Tamil Nadu, India*

Prajisha Jayaprakash − *Structural Biology and Bio-Computing Laboratory, Department of Bioinformatics, Science Block, Alagappa University, Karaikudi 630 004 Tamil Nadu, India*

Suresh Kumar Rayala − *Department of Biotechnology, Indian Institute of Technology Madras, Chennai 600 036 Tamil Nadu, India*

Ganesh Venkatraman − *Department of Human Genetics, College of Biomedical Sciences, Sri Ramachandra University, Chennai 600 116 Tamil Nadu, India*

Raghu Rangaswamy − *Structural Biology and Bio-Computing Laboratory, Department of Bioinformatics, Science Block, Alagappa University, Karaikudi 630 004 Tamil Nadu, India*

Complete contact information is available at: https://pubs.acs.org/10.1021/acsomega.1c02032

Author Contributions

J.J. is the corresponding author and has helped in the design and guidance of work. S.K.R. and G.V. helped with the target

https://doi.org/10.1021/acsomega.1c02032
ACS Omega 2021, 6, 26829−26845

identification and addressed the problems associated with it. J.B. designed and performed the work and wrote the manuscript. P.J. and R.R. helped in data collection.

Notes

The authors declare no competing financial interest.

■ ACKNOWLEDGMENTS

J.J. thanks the DST-INDO TAIWAN (GITA/DST/TWN/P-86/2019 dated: 04.03.2020), Board of Research in Nuclear Sciences (BRNS) (35/14/ 02/2018 BRNS/35009), DST—Fund for Improvement of S&T Infrastructure in Universities & Higher Educational Institutions (FIST) (SR/FST/LSI-667/2016) (C) and DST-Promotion of University Research and Scientific Excellence (PURSE) (No. SR/PURSE Phase 2/38) (G), 2017. J.B. is grateful to the UGC OBC National Fellowship (F./2015-16/NFO-2015-17-OBC-PON-29027). Special thanks go to Dr. Pritesh Bhat, Principal Scientist, Schrödinger, and Dr. Koushik Kasavajhala, Senior Scientist I, Schrödinger, for their timely help, views, and suggestions to carry out this work.

■ LIST OF ABBREVIATIONS

ABPS	Adaptive Poisson Boltzmann Solver
AID	auto-inhibitory domain
B3LYP	Becke, 3 parameter, Lee−Yang−Parr
BTK	Bruton Tyrosine Kinase inhibitor
CADD	computer-aided drug design
Cdc42/Rac1	cell division control protein 42/Ras-related C3 botulinum toxin substrate 1
CRIB	Cdc42/Rac1 interactive binding domain
DFT	density functional theory
(M) ESP	molecular electrostatic potential
FDA	Food and Drug Administration
FMO	frontier molecular orbital
HDI	human development index
HOMO	highest occupied molecular orbital
HS	hydration site
HTVS	high-throughput virtual screening
IARC	International Agency for Research and Cancer
KD	kinase domain
LUMO	lowest unoccupied molecular orbital
MD	molecular dynamics
OPLS	optimized potential for liquid simulation
PAK	p21-activated kinase
RMSD	root-mean-square deviation
RMSF	root-mean-square fluctuation
SBVS	structure-based virtual screening
SPC	simple point charge
SP	standard precision
WM	WaterMap
XP	extra precision

■ REFERENCES

(1) T.I.A.f.R.o.C. (IARC). Latest Global Cancer Data (IARC) 2018, Press release no263.

(2) Mottini, C.; Napolitano, F.; Li, Z.; Gao, X.; Cardone, L. Computer-aided drug repurposing for cancer therapy: Approaches and opportunities to challenge anticancer targets. *Semin Cancer Biol.* **2021**, *68*, 59−74.

(3) Bray, F.; Jemal, A.; Grey, N.; Ferlay, J.; Forman, D. Global cancer transitions according to the, human development index (2008−2030): a population-based study. *Lancet Oncol.* **2012**, *13*, 790−801.

(4) Wong, C. H.; Siah, K. W.; Lo, A. W. Estimation of clinical trial success rates and related parameters. *Biostatistics* **2019**, *20*, 273−286.

(5) Aier, I.; Varadwaj, P. K. Drug Repositioning: Principles, Resources, and Application of Structure-Based Virtual Screening for the Identification of Anticancer Agents. In *Molecular Docking for Computer-Aided Drug Design*, 1st ed.; Academic Press, 2021; pp 313−336.

(6) Shih, H. P.; Zhang, X.; Aronov, A. M. Drug discovery effectiveness from the standpoint of therapeutic mechanisms and indications. *Nat. Rev. Drug Discovery* **2018**, *17*, 19−33.

(7) Patel, D. D.; Antoni, C.; Freedman, S. J.; Levesque, M. C.; Sundy, J. S. Phase 2 to phase 3 clinical trial transitions: reasons for success and failure in immunologic diseases. *J. Allergy Clin. Immunol.* **2017**, *140*, 685−687.

(8) Tanoli, Z.; Vähä-Koskela, M.; Aittokallio, T. Artificial intelligence, machine learning, and drug repurposing in cancer. *Expert. Opin. Drug Discovery* **2021**, 1−13.

(9) Ashburn, T. T.; Thor, K. B. Drug repositioning: identifying and developing new uses for existing drugs. *Nat. Rev. Drug Discovery* **2004**, *3*, 673−683.

(10) Park, K. A review of computational drug repurposing. *Transl. Clin. Pharmacol.* **2019**, *27*, 59−63.

(11) Ekins, S.; Williams, A. J.; Krasowski, M. D.; Freundlich, J. S. *In silico* repositioning of approved drugs for rare and neglected diseases. *Drug Discovery Today* **2011**, *16*, 298−310.

(12) Hou, J.; Wang, D.; Zhang, R.; Wang, H. Experimental therapy of hepatoma with artemisinin and its derivatives: *in vitro* and *in vivo* activity, chemosensitization, and mechanisms of action. *Clin. Cancer Res.* **2008**, *14*, 5519−5530.

(13) Shim, J. S.; Liu, J. O. Recent advances in drug repositioning for the discovery of new anticancer drugs. *Int. J. Biol. Sci.* **2014**, *10*, 654−663.

(14) Chateauvieux, S.; Morceau, F.; Dicato, M.; Diederich, M. Molecular and therapeutic potential and toxicity of valproic acid. *J. Biomed. Biotechnol.* **2010**, *2010*, 1−18.

(15) Tsubamoto, H.; Sonoda, T.; Inoue, K. Impact of itraconazole on the survival of heavily pre-treated patients with triple-negative breast cancer. *Anticancer. Res.* **2014**, *34*, 3839−3844.

(16) Martino, S.; Cauley, J. A.; Barrett-Connor, E.; Powles, T. J.; Mershon, J.; Disch, D.; Secrest, R. J.; Cummings, S. R. Continuing outcomes relevant to Evista: breast cancer incidence in postmenopausal osteoporotic women in a randomized trial of raloxifene. *J. Natl. Cancer Inst.* **2004**, *96*, 1751−1761.

(17) Singhal, S.; Mehta, J. Thalidomide in cancer. *Biomed. Pharmacother.* **2002**, *56*, 4−12.

(18) Penas-Prado, M.; Hess, K. R.; Fisch, M. J.; Lagrone, L. W.; Groves, M. D.; Levin, V. A.; De Groot, J. F.; Puduvalli, V. K.; Colman, H.; Volas-Redd, G.; Giglio, P.; Conrad, C. A.; Salacz, M. E.; Floyd, J. D.; Loghin, M. E.; Hsu, S. H.; Gonzalez, J.; Chang, E. L.; Woo, S. Y.; Mahajan, A.; Aldape, K. D.; Yung, W. K.; Gilbert, M. R. Randomized phase II adjuvant factorial study of dose-dense temozolomide alone and in combination with isotretinoin, celecoxib, and/or thalidomide for glioblastoma. *Neuro-Oncology* **2015**, *17*, 266−273.

(19) Phillips, I.; Langley, R.; Gilbert, D.; Ring, A. Aspirin as a treatment for cancer. *Clin. Oncol.* **2013**, *25*, 333−335.

(20) Thorat, M. A.; Cuzick, J. Role of aspirin in cancer prevention. *Curr. Oncol. Rep.* **2013**, *15*, 533−540.

(21) Kim, C. K.; Joe, Y. A.; Lee, S.-K.; Kim, E.-K.; Eunju, O.; Kim, H.-K.; Oh, B. J.; Hong, S. H.; Hong, Y.-K. Enhancement of anti-tumor activity by low-dose combination of the recombinant urokinase kringle domain and celecoxib in a glioma model. *Cancer Lett.* **2010**, *288*, 251−260.

(22) Del Barco, S.; Vazquez-Martin, A.; Cufí, S.; Oliveras-Ferraros, C.; Bosch-Barrera, J.; Joven, J.; Martin-Castillo, B.; Menendez, J. A. Metformin: multi-faceted protection against cancer. *Oncotarget* **2011**, *2*, 896−917.

(23) Lin, S. Y.; Chang, H. H.; Lai, Y. H.; Lin, C. H.; Chen, M. H.; Chang, G. C.; Tsai, M. F.; Chen, J. J. Digoxin suppresses tumor

https://doi.org/10.1021/acsomega.1c02032
ACS Omega 2021, 6, 26829−26845

malignancy through inhibiting multiple Src-related signaling pathways in non-small cell lung cancer. *PLoS One* **2015**, *10*, No. e0123305.
(24) Shim, J. S.; Matsui, Y.; Bhat, S.; Nacev, B. A.; Xu, J.; Bhang, H. E.; Dhara, S.; Han, K. C.; Chong, C. R.; Pomper, M. G.; So, A.; Liu, J. O. Effect of nitroxoline on angiogenesis and growth of human bladder cancer. *J. Natl. Cancer Inst.* **2010**, *102*, 1855−1873.
(25) Sleire, L.; Førde, H. E.; Netland, I. A.; Leiss, L.; Skeie, B. S.; Enger, P. Ø. Drug repurposing in cancer. *Pharmacol. Res.* **2017**, *124*, 74−91.
(26) Würth, R.; Thellung, S.; Bajetto, A.; Mazzanti, M.; Florio, T.; Barbieri, F. Drug-repositioning opportunities for cancer therapy: novel molecular targets for known molecules. *Drug Discovery Today* **2016**, *21*, 190−199.
(27) Parvathaneni, V.; Kulkarni, N. S.; Muth, A.; Gupta, V. Drug repurposing: a promising tool to accelerate the drug discovery process. *Drug Discovery Today* **2019**, *24*, 2076−2085.
(28) Gupta, S. C.; Sung, B.; Prasad, S.; Webb, L. J.; Aggarwal, B. B. Cancer drug discovery by repurposing: teaching new tricks to old dogs. *Trends Pharmacol. Sci.* **2013**, *34*, 508−517.
(29) Agrawal, P. Advantages and challenges in drug re-profiling. *J. Pharmacovigilance* **2015**, *S2*, No. e002.
(30) Shih, H. P.; Zhang, X.; Aronov, A. M. Drug discovery effectiveness from the standpoint of therapeutic mechanisms and indications. *Nat. Rev. Drug Discovery* **2018**, *17*, 19−33.
(31) Palve, V.; Liao, Y.; Remsing Rix, L. L.; Rix, U. Turning liabilities into opportunities: Off-target based drug repurposing in cancer. *Semin. Cancer Biol.* **2021**, *68*, 209−229.
(32) Pahud, D.; Mitchell, L.; Wilbbanks, J.; Stevens, M.; Weir, S.; McBride, J.; Portilla, L.; Ling, S.; Pezala, Ed.; Nameth, M.; O'Donoghue, B.; Rai, A.; Lappin, D.; Ogle, M.; Howell, S. A new market access path for repurposed drugs. https://www.kauffman.org/what-we-do/research/2014/05/a-new-market-access-path-for-repurposed-drugs (accessed May 14, 2014).
(33) Adams, J. A. Kinetic and catalytic mechanisms of protein kinases. *Chem Rev.* **2001**, *101*, 2271−2290.
(34) Rask-Andersen, M.; Zhang, J.; Fabbro, D.; Schiöth, H. B. Advances in kinase targeting: current clinical use and clinical trials. *Trends Pharmacol. Sci.* **2014**, *35*, 604−620.
(35) Wu, P.; Nielsen, T. E.; Clausen, M. H. FDA-approved small-molecule kinase inhibitors. *Trends Pharmacol. Sci.* **2015**, *36*, 422−439.
(36) Zhang, J.; Yang, P. L.; Gray, N. S. Targeting cancer with small molecule kinase inhibitors. *Nat. Rev. Cancer* **2009**, *9*, 28−39.
(37) Lei, M.; Robinson, M. A.; Harrison, S. C. The active conformation of the PAK1 kinase domain. *Structure* **2005**, *13*, 769−778.
(38) Zenke, F. T.; King, C. C.; Bohl, B. P.; Bokoch, G. M. Identification of a central phosphorylation site in p21-activated kinase regulating autoinhibition and kinase activity. *J. Biol. Chem.* **1999**, *274*, 32565−32573.
(39) Vadlamudi, R. K.; Kumar, R. P21-activated kinases in human cancer. *Cancer Metastasis Rev.* **2003**, *22*, 385−393.
(40) Meng, J.; Meng, Y.; Hanna, A.; Janus, C.; Jia, Z. Abnormal long-lasting synaptic plasticity and cognition in mice lacking the mental retardation gene Pak3. *J. Neurosci.* **2005**, *25*, 6641−6650.
(41) Kichina, J. V.; Goc, A.; Al-Husein, B.; Somanath, P. R.; Kandel, E. S. PAK1 as a therapeutic target. *Expert Opin. Ther. Targets* **2010**, *14*, 703−725.
(42) Hao, C.; Zhao, F.; Song, H.; Guo, J.; Li, X.; Jiang, X.; Huan, R.; Song, S.; Zhang, Q.; Wang, R.; Wang, K.; Pang, Y.; Liu, T.; Lu, T.; Huang, W.; Wang, J.; Lin, B.; He, Z.; Li, H.; Li, F.; Zhao, D.; Cheng, M. Structure-Based Design of 6-Chloro-4-aminoquinazoline-2-carboxamide Derivatives as Potent and Selective p21-Activated Kinase 4 (PAK4) Inhibitors. *J. Med. Chem.* **2018**, *61*, 265−285.
(43) Semenova, G.; Chernoff, J. Targeting PAK1. *Biochem. Soc. Trans.* **2017**, *45*, 79−88.
(44) Gul, M.; Fakhar, M.; Najumuddin; Rashid, S. Phosphorylation-dependent activity-based conformational changes in P21-activated kinase family members and screening of novel ATP competitive inhibitors. *PLoS One* **2019**, *14*, No. e0225132.
(45) Bowen, L. R.; Li, D. J.; Nola, D. T.; Anderson, M. O.; Heying, M.; Groves, A. T.; Eagon, S. Identification of potential Zika virus NS2B-NS3 protease inhibitors via docking, molecular dynamics and consensus scoring-based virtual screening. *J. Mol. Model.* **2019**, *25*, No. 194.
(46) Senapedis, W.; Crochiere, M.; Baloglu, E.; Landesman, Y. Therapeutic Potential of Targeting PAK Signaling. *Anti-Cancer Agents Med. Chem.* **2015**, *16*, 75−88.
(47) Wishart, D. S.; Feunang, Y. D.; Guo, A. C.; Lo, E. J.; Marcu, A.; Grant, J. R.; Sajed, T.; Johnson, D.; Li, C.; Sayeeda, Z.; Assempour, N.; Iynkkaran, I.; Liu, Y.; Maciejewski, A.; Gale, N.; Wilson, A.; Chin, L.; Cummings, R.; Le, D.; Pon, A.; Knox, C.; Wilson, M. DrugBank 5.0: a major update to the DrugBank database for 2018. *Nucleic Acids Res.* **2018**, *46*, D1074−D1082.
(48) Biswal, J.; Jayaprakash, P.; Suresh Kumar, R.; Venkatraman, G.; Poopandi, S.; Rangasamy, R.; Jeyaraman, J. Identification of PAK1 inhibitors using water thermodynamic analysis. *J. Biomol. Struct. Dyn.* **2020**, *38*, 13−31.
(49) Ma, D. L.; Chan, D. S.; Leung, C. H. Drug repositioning by structure-based virtual screening. *Chem. Soc. Rev.* **2013**, *42*, 2130−2141.
(50) Abel, R.; Young, T.; Farid, R.; Berne, B. J.; Friesner, R. A. The role of the active site solvent in the thermodynamics of factor Xa-ligand binding. *J. Am. Chem. Soc.* **2008**, *130*, 2817−2831.
(51) Friesner, R. A.; Murphy, R. B.; Repasky, M. P.; Frye, L. L.; Greenwood, J. R.; Halgren, T. A.; Sanschagrin, P. C.; Mainz, D. T. Extra Precision Glide: Docking and scoring incorporating a Model of Hydrophobic Enclosure for Protein-Ligand Complexes. *J. Med. Chem.* **2006**, *49*, 6177−6196.
(52) Beuming, T.; Farid, R.; Sherman, W. High-energy water sites determine peptide binding affinity and specificity of PDZ domains. *Protein Sci.* **2009**, *18*, 1609−1619.
(53) Biswal, J.; Prajisha, J.; Rayala, S. K.; Venkatraman, G.; Rangasamy, R.; Poopandi, S.; Jeyaraman, J. Water Mapping and Scoring approaches to predict the role of Hydration sites in Binding Affinity of PAK1 inhibitors. *Comb. Chem. High Throughput Screening* **2021**, *24*, 1.
(54) Abel, R.; Salam, N. K.; Shelley, J.; Farid, R.; Friesner, R. A.; Sherman, W. Contribution of explicit solvent effects to the binding affinity of small-molecule inhibitors in blood coagulation factor serine proteases. *Chem. Med. Chem.* **2011**, *6*, 1049−1066.
(55) Robinson, D. D.; Sherman, W.; Farid, R. Understanding kinase selectivity through energetic analmaysis of binding site waters. *ChemMedChem* **2010**, *5*, 618−627.
(56) Geschwindner, S.; Ulander, J. The current impact of water thermodynamics for small-molecule drug discovery. *Expert Opin. Drug Discovery* **2019**, *14*, 1221−1225.
(57) Haider, K.; Huggins, D. J. Combining Solvent Thermodynamic Profiles with Functionality Maps of the Hsp90 Binding Site to Predict the Displacement of Water Molecules. *J. Chem. Inf. Model.* **2013**, *53*, 2571−2586.
(58) Bucher, D.; Stouten, P.; Triballeau, N. Shedding Light on Important Waters for Drug Design: Simulations versus Grid-Based Methods. *J. Chem. Inf. Model.* **2018**, *58*, 692−699.
(59) Sohraby, F.; Bagheri, M.; Aryapour, H. Performing an *In Silico* Repurposing of Existing Repurposing of Existing Drugs by Combining Virtual Screening and Molecular Dynamics Simulation. In *Computational Methods for Drug Repurposing*; Humana Press, 2019; Vol. *19*, pp 23−43.
(60) Dighe, S. N.; Deora, G. S.; De la Mora, E.; Nachon, F.; Chan, S.; Parat, M. O.; Brazzolotto, X.; Ross, B. P. Discovery and Structure-Activity Relationships of a Highly Selective Butyrylcholinesterase Inhibitor by Structure-Based Virtual Screening. *J. Med. Chem.* **2016**, *59*, 7683−7689.
(61) Halgren, T. A.; Murphy, R. B.; Friesner, R. A.; Beard, H. S.; Frye, L. L.; Pollard, W. T.; Banks, J. L. Glide: A New Approach for Rapid, Accurate Docking and Scoring. 2. Enrichment Factors in Database Screening. *J. Med. Chem.* **2004**, *47*, 1750−1759.

https://doi.org/10.1021/acsomega.1c02032
ACS Omega 2021, 6, 26829−26845

(62) Friesner, R. A.; Murphy, R. B.; Repasky, M. P.; Frye, L. L.; Greenwood, J. R.; Halgren, T. A.; Sanschagrin, P. C.; Mainz, D. T. Extra Precision Glide: Docking and Scoring Incorporating a Model of Hydrophobic Enclosure for Protein-Ligand Complexes. *J. Med. Chem.* **2006**, *49*, 6177−6196.
(63) Shah, F.; Gut, J.; Legac, J.; Shivakumar, D.; Sherman, W.; Rosenthal, P. J.; Avery, M. A. Computer-aided drug design of falcipain inhibitors: virtual screening, structure-activity relationships, hydration site thermodynamics, and reactivity analysis. *J. Chem. Inf. Model.* **2012**, *52*, 696−710.
(64) Cappel, D.; Sherman, W.; Beuming, T. Calculating Water Thermodynamics in the Binding Site of Proteins - Applications of WaterMap to Drug Discovery. *Curr. Top. Med. Chem.* **2017**, *17*, 2586−2598.
(65) Pearlstein, R. A.; Hu, Q. Y.; Zhou, J.; Yowe, D.; Levell, J.; Dale, B.; Kaushik, V. K.; Daniels, D.; Hanrahan, S.; Sherman, W.; Abel, R. New hypotheses about the structure-function of proprotein convertase subtilisin/kexin type 9: analysis of the epidermal growth factor-like repeat a docking site using WaterMap. *Proteins: Struct., Funct., Bioinf.* **2010**, *78*, 2571−2586.
(66) Hajihassan, Z.; Rabbani-Chadegani, A. Studies on the binding affinity of anticancer drug mitoxantrone to chromatin, DNA and histone proteins. *J. Biomed. Sci.* **2009**, *16*, 31.
(67) Opie, L. H. Role of vasodilation in the antihypertensive and antianginal effects of labetalol:implications for therapy of combined hypertension and angina. *Cardiovasc. Drug Ther.* **1988**, *2*, 369−376.
(68) Wu, J.; Zhang, M.; Liu, D. Acalabrutinib (ACP-196): a selective second-generation BTK inhibitor. *J. Hematol. Oncol.* **2016**, *9*, No. 21.
(69) Mills, J.; Vardeny, O. The Role of Neprilysin Inhibitors in Cardiovascular Disease. *Curr. Heart Failure Rep.* **2015**, *12*, 389−394.
(70) Shrestha, M.; Keyes, D. C. Anthelmintics. In *Haddad and Winchester's Clinical Management of Poisoning and Drug Overdose*, 4th ed.; Elsevier, 2007.
(71) Fagiolini, A.; Comandini, A.; Catena Dell'Osso, M.; Kasper, S. Rediscovering trazodone for the treatment of major depressive disorder. *CNS Drugs* **2012**, *26*, 1033−1049.
(72) Chen, A. PARP inhibitors: its role in treatment of cancer. *Chin. J. Cancer* **2011**, *30*, 463−471.
(73) Knegtel, R. M.; Robinson, D. D. A Role for Hydration in Interleukin-2 Inducible T Cell Kinase (Itk) Selectivity. *Mol. Inf.* **2011**, *30*, 950−959.
(74) Licciulli, S.; Maksimoska, J.; Zhou, C.; Troutman, S.; Kota, S.; Liu, Q.; Duron, S.; Campbell, D.; Chernoff, J.; Field, J.; Marmorstein, R.; Kissil, J. L. FRAX597, a small molecule inhibitor of the p21-activated kinases, inhibits tumorigenesis of neurofibromatosis type 2 (NF2)-associated Schwannomas. *J. Biol. Chem.* **2013**, *288*, 29105−29114.
(75) Ndubaku, C. O.; Crawford, J. J.; Drobnick, J.; Aliagas, I.; Campbell, D.; Dong, P.; Dornan, L. M.; Duron, S.; Epler, J.; Gazzard, L.; Heise, C. E.; Hoeflich, K. P.; Jakubiak, D.; La, H.; Lee, W.; Lin, B.; Lyssikatos, J. P.; Maksimoska, J.; Marmorstein, R.; Murray, L. J.; O'Brien, T.; Oh, A.; Ramaswamy, S.; Wang, W.; Zhao, X.; Zhong, Y.; Blackwood, E.; Rudolph, J. Design of Selective PAK1 Inhibitor G-5555: Improving Properties by Employing an Unorthodox Low-pK a Polar Moiety. *ACS. Med. Chem. Lett.* **2015**, *6*, 1241−1246.
(76) Rudolph, J.; Murray, L. J.; Ndubaku, C. O.; O'Brien, T.; Blackwood, E.; Wang, W.; Aliagas, I.; Gazzard, L.; Crawford, J. J.; Drobnick, J.; Lee, W.; Zhao, X.; Hoeflich, K. P.; Favor, D. A.; Dong, P.; Zhang, H.; Heise, C. E.; Oh, A.; Ong, C. C.; La, H.; Chakravarty, P.; Chan, C.; Jakubiak, D.; Epler, J.; Ramaswamy, S.; Vega, R.; Cain, G.; Diaz, D.; Zhong, Y. Chemically diverse Group-I p21-activated kinase (PAK) inhibitors impart acute cardiovascular toxicity with a narrow therapeutic window. *J. Med. Chem.* **2016**, *59*, 5520−5541.
(77) McCoull, W.; Hennessy, E. J.; Blades, K.; Chuaqui, C.; Dowling, J. E.; Ferguson, A. D.; Goldberg, F. W.; Howe, N.; Jones, C. R.; Kemmitt, P. D.; Lamont, G.; Varnes, J. G.; Ward, R. A.; Yang, B. Optimization of Highly Kinase Selective Bis-anilino Pyrimidine PAK1 Inhibitors. *ACS. Med. Chem. Lett.* **2016**, *7*, 1118−1123.
(78) Fleming, I. *Molecular Orbitals and Organic Chemicals Reactions: Student Edition*; John Wilsey & Sons, Ltd: Chichester, 2009.
(79) Wakchaure, P. D.; Ghosh, S.; Ganguly, B. Revealing the Inhibition Mechanism of RNA-Dependent RNA Polymerase (RdRp) of SARS-CoV-2 by Remdesivir and Nucleotide Analogues: A Molecular Dynamics Simulation Study. *J. Phys. Chem. B* **2020**, *124*, 10641−10652.
(80) Hussain, A. S.; Shanthi, V.; Sheik, S. S.; Jeyakanthan, J.; Selvarani, P.; Sekar, K. PDB Goodies–a web-based GUI to manipulate the Protein Data Bank file. *Acta Crystallogr., Sect. D: Biol. Crystallogr.* **2002**, *58*, 1385−1386.
(81) *Schrödinger Release 2017: Protein Preparation Wizard*; Epik, Schrödinger, LLC: New York, NY, 2017. *Impact*; Schrödinger, LLC: New York, NY, 2017. *Prime*; Schrödinger, LLC: New York, NY, 2017.
(82) Sastry, G. M.; Adzhigirey, M.; Day, T.; Annabhimoju, R.; Sherman, W. Protein and ligand preparation: Parameters, protocols, and influence on virtual screening enrichments. *J. Comput.-Aided Mol. Des.* **2013**, *27*, 221−234.
(83) Rostkowski, M.; Olsson, M. H.; Søndergaard, C. R.; Jensen, J. H. Graphical analysis of pH-dependent properties of proteins predicted using PROPKA. *BMC Struct. Biol.* **2011**, *11*, No. 6.
(84) Jorgensen, W. L.; Maxwell, D. S.; Tirado-Rives, J. Development and testing of the OPLS all-atom force field on conformational energetic and properties of organic liquids. *J. Am. Chem. Soc.* **1996**, *118*, 11225−11236.
(85) Choubey, S. K.; Jeyaraman, J. A mechanistic approach to explore novel HDAC1 inhibitor using pharmacophore modelling 3D-QSAR analysis, molecular docking, density functional and molecular dynamics simulation study. *J. Mol. Graphics Modell.* **2016**, *70*, 54−69.
(86) *Schrödinger Release 2017: LigPrep*; Schrödinger, LLC: New York, NY, 2017.
(87) Harder, E.; Damm, W.; Maple, J.; Wu, C.; Reboul, M.; Xiang, J. Y.; Wang, L.; Lupyan, D.; Dahlgren, M. K.; Knight, J. L.; Kaus, J. W.; Cerutti, D.; Krilov, G.; Jorgensen, W. L.; Abel, R.; Friesner, R. A. OPLS3: a force field providing broad coverage of drug-like small molecules and proteins. *J. Chem. Theory Comput.* **2016**, *12*, 281−296.
(88) Friesner, R. A.; Banks, J. L.; Murphy, R. B.; Halgren, T. A.; Klicic, J. J.; Mainz, D. T.; Repasky, M. P.; Knoll, E. H.; Shelley, M.; Perry, J. K.; Shaw, D. E.; Francis, P.; Shenkin, P. S. Glide: a new approach for rapid, accurate docking and scoring. 1. Method and assessment of docking accuracy. *J. Med. Chem.* **2004**, *47*, 1739−1749.
(89) Surekha, K.; Prabhu, D.; Richard, M.; Nachiappan, M.; Biswal, J.; Jeyakanthan, J. Investigation of vital pathogenic target orotate phosphoribosyltransferases (OPRTase) from *Thermus thermophilus* HB8: Phylogenetic and molecular modelling approach. *Gene.* **2016**, *583*, 102−111.
(90) Matter, H.; Güssregen, S. Characterizing hydration sites in protein-ligand complexes towards the design of novel ligands. *Bioorg. Med. Chem. Lett.* **2018**, *28*, 2343−2352.
(91) Young, T.; Abel, R.; Kim, B.; Berne, B. J.; Friesner, R. A. Motifs for molecular recognition exploiting hydrophobic enclosure in protein-ligand binding. *Proc. Natl. Acad. Sci. U.S.A.* **2007**, *104*, 808−813.
(92) Weldon, D. J.; Shah, F.; Chittiboyina, A. G.; Sheri, A.; Chada, R. R.; Gut, J.; Rosenthal, P. J.; Shivakumar, D.; Sherman, W.; Desai, P.; Jung, J. C.; Avery, M. A. Synthesis, biological evaluation, hydration site thermodynamics, and chemical reactivity analysis of α-keto substituted peptidomimetics for the inhibition of Plasmodium falciparum. *Bioorg. Med. Chem. Lett.* **2014**, *24*, 1274−1279.
(93) Horbert, R.; Pinchuk, B.; Johannes, E.; Schlosser, J.; Schmidt, D.; Cappel, D.; Totzke, F.; Schächtele, C.; Peifer, C. Optimization of potent DFG-in inhibitors of platelet derived growth factor receptorβ (PDGF-Rβ) guided by water thermodynamics. *J. Med. Chem.* **2015**, *58*, 170−182.
(94) Mondal, J.; Friesner, R. A.; Berne, B. J. Role of Desolvation in Thermodynamics and Kinetics of Ligand Binding to a kinase. *J. Chem. Theory Comput.* **2014**, *10*, 5696−5705.
(95) Beuming, T.; Che, Y.; Abel, R.; Kim, B.; Shanmugasundaram, V.; Sherman, W. Thermodynamic analysis of water molecules at the

https://doi.org/10.1021/acsomega.1c02032
ACS Omega 2021, 6, 26829−26845

surface of proteins and applications to binding site prediction and characterization. *Proteins: Struct.,Funct., Bioinf.* **2012**, *80*, 871−883.
(96) *Schrödinger Release 2021-3: Jaguar*; Schrödinger, LLC: New York, NY, 2021.
(97) Bochevarov, A. D.; Edward, H.; Hughes, T. F.; Greenwood, J. R.; Braden, D. A.; Philipp, D. M.; Rinaldo, D.; Halls, M. D.; Zhang, J.; Friesner, R. A. Jaguar: A high-performance quantum chemistry software program with strengths in life and materials sciences. *Int. J. Quantum. Chem.* **2013**, *113*, 2110−2142.
(98) Prajisha, J.; Biswal, J.; Jeyakanthan, J. Discovery of potent Camkk1 kinase inhibitors through e-pharmacophore and molecular screening approaches. *J. Biomol. Struct. Dyn.* **2020**, *26*, 1−17.
(99) Grant, J. A.; Pickup, B. T.; Nicholls, A. A Smooth permittivity functions for Poisson-Boltzmann Solvation Methods. *J. Comput. Chem.* **2001**, *22*, 608−640.
(100) Konecny, R.; Baker, N. A.; McCammon, J. A. iAPBS: a programming interface to the adaptive poisson-Boltzmann solver. *Comput. Sci. Discovery* **2012**, *5*, No. 015005.
(101) Lerner, M. G. *Carlson, HA-Ann Arbor*; University of Michigan, 2006.
(102) Baker, N. A.; Sept, D.; Joseph, S.; Holst, M. J.; McCammon, J. A. Electrostatics of nanosystems: application to microtubules and the ribosome. *Proc. Natl. Acad. Sci. U.S.A.* **2001**, *98*, 10037−10041.
(103) *Schrödinger Release 2017: Desmond Molecular Dynamics System*; D. E. Shaw Research: New York, NY, 2017.
(104) Martyna, G. J.; Klein, M. L.; Tuckerman, M. Nosé-Hoover chains: The canonical ensemble via continuous dynamics. *J. Chem. Phys.* **1992**, *97*, 2635−2643.
(105) Miyamoto, S.; Kollman, P. A. Settle: An Analytical Version of the SHAKE and RATTLE Algorithm for Rigid Water Models. *J. Comput. Chem.* **1992**, *13*, 952−962.
(106) Toukmaji, A. Y.; Board, J. A., Jr. Ewald Summation Techniques in Perspective: A Survey. *Comput. Phys. Commun.* **1996**, *95*, 73−92.
(107) Wang, J.; Wu, J. W.; Wang, Z. X. Structural insights into the autoactivation mechanism of p21-activated protein kinase. *Structure* **2011**, *19*, 1752−1761.

https://doi.org/10.1021/acsomega.1c02032
ACS Omega 2021, 6, 26829−26845